Semi-empirical white dwarf initial-final mass relationships: a thorough analysis of systematic uncertainties due to stellar evolution models

Maurizio Salaris[1]

Astrophysics Research Institute, Liverpool John Moores University, Twelve Quays House, Egerton Wharf, Birkenhead CH41 1LD, UK

ms@astro.livjm.ac.uk

and

Aldo Serenelli[1]

Institute for Advanced Study, Einstein Drive, Princeton, NJ 08540, USA

and

Achim Weiss

Max-Planck-Institut für Astrophysik, Karl-Schwarzschild-Str. 1, 85748 Garching, Germany

and

Marcelo Miller Bertolami[2]

Facultad de Ciencias Astronómicas y Geofísicas, Universidad Nacional de La Plata, Paseo del Bosque S/N, (1900) La Plata, Argentina

ABSTRACT

Using the most recent results about white dwarfs in 10 open clusters, we revisit semi-empirical estimates of the initial-final mass relation in star clusters, with emphasis on the use of stellar evolution models. We discuss the influence of these models on each step of the derivation. One intention of our work is to use consistent sets of calculations both for the isochrones and the white dwarf

---

[1]Max-Planck-Institut für Astrophysik, Karl-Schwarzschild-Str. 1, 85748 Garching, Germany

[2]IALP-CONICET, La Plata, Argentina

cooling tracks. The second one is to derive the range of systematic errors arising from stellar evolution theory. This is achieved by using different sources for the stellar models and by varying physical assumptions and input data. We find that systematic errors, including the determination of the cluster age, are dominating the initial mass values, while observational uncertainties influence the final mass primarily. After having determined the systematic errors, the initial-final mass relation allows us finally to draw conclusions about the physics of the stellar models, in particular about convective overshooting.

Subject headings: stars: AGB and post-AGB — stars: evolution — stars: individual(Sirius) — stars: mass loss — white dwarfs — open clusters and associations: individual (Pleiades, Hyades, Praesepe, NGC1039, NGC2168, NGC2099, NGC2516, NGC3532, NGC6819, NGC7789)

1. Introduction

The initial-final mass relation (IFMR) for low- and intermediate-mass stars is an important input for many astrophysical problems. Given the initial Main Sequence (MS) mass of a formed star, the IFMR provides the expected mass during its final White Dwarf (WD) cooling stage, and is an estimate of the total mass lost by the star during its evolutionary history. A correct assessment of the IFMR is very important when predicting, for example, the chemical evolution history of stellar populations, or their mass-to-light ratio (defined as the ratio of the mass of evolving stars plus remnants – WDs, neutron stars and black holes – to the integrated luminosity of the population), and in general for any problem related to the origin and evolution of gas in stellar populations. It is also a crucial item when using the WD luminosity functions to determine the age of stellar populations (see, e.g., Prada Moroni & Straniero 2007). It also provides an empirical test concerning the upper initial mass value M_{up} of stars developing degenerate carbon-oxygen cores, and thus a lower limit of the mass range of core-collapse supernovae. For a thorough review of the history of the IFMR, we recommend Weidemann (2000).

Theoretical estimates of the IFMR are still prone to large uncertainties. This is due to our poor knowledge of the efficiency of mass loss processes for low- and intermediate-mass stars but also to uncertainties in the predicted size of CO cores during the Asymptotic Giant Branch (AGB) evolution, resulting mainly from uncertainties in the treatment of the thermal pulse phase, with the associated third dredge-up, hot bottom burning (see, e.g., Iben & Renzini 1983) and also the treatment of rotation (Dominguez et al. 1996). In fact, the recognition that intermediate-mass stars may lose the largest part of their mass during

the AGB phase stems from early IFMRs (Koester & Weidemann 1980).

Starting with the pioneering work by Weidemann (1977), (semi-)empirical routes have been followed to establish the IFMR independently of theoretical modelling the AGB phase, leading to a series of global determinations of the IFMR by, e.g., Weidemann & Koester (1983), Weidemann (1987), Weidemann (2000), Ferrario et al. (2005), and many others.

Methods to estimate the IFMR that make use of the smallest number of assumptions are probably those based on the use of WDs harbored in star clusters (but see also Catalán et al. 2008b, for a very recent study of the IFMR based on WDs in common proper motion pairs). Thanks to a large amount of observational effort by various authors (see, e.g. Koester & Reimers 1993, 1996; Claver et al. 2001; Dobbie et al. 2004; Kalirai et al. 2005; Barstow et al. 2005; Dobbie et al. 2006a) the recent study of the IFMR by Ferrario et al. (2005) makes use of 40 DA (hydrogen-atmosphere) WDs belonging to 7 open clusters. Even more recently Kalirai et al. (2008) have added a few more data points below the low-mass end (initial masses below $\sim 2.0\ M_\odot$) of the Ferrario et al. (2005) sample, by including WDs detected in the old open clusters NGC6819, NGC7789 and NGC6791, while Rubin et al. (2008) have provided WD data for the ~ 200 Myr old cluster NGC1039. Therefore, the observational material is increasingly covering not only more objects, but also a larger range of cluster – and thus WD – ages and metallicities, such that even differential investigations may become feasible in the near future. At the same time, high-resolution, high signal-to-noise spectra and improved spectral analysis methods reduce the intrinsic errors in the determination of the WD masses. It is therefore time to investigate the systematic errors arising from stellar evolution theory and models that enter these semi-empirical methods. This is the main object of this work.

IFMR determinations based on cluster WDs work as follows: after detection, spectroscopic estimates of the WD surface gravity g and $T_{\rm eff}$ are needed. For a fixed g-$T_{\rm eff}$ pair, interpolation within a grid of theoretical WD models covering a range of masses provides the mass $M_{\rm f}$ and the age $t_{\rm cool}$ of the WD. Independent theoretical isochrone fits to the Turn Off (TO) luminosity in the cluster Color-Magnitude-Diagram (CMD) provide an estimate of the cluster age $t_{\rm clus}$. The difference $t_{\rm clus} - t_{\rm cool}$ is equal to the lifetime $t_{\rm prog}$ of the WD progenitor, from the MS until the start of the WD cooling. Making use of mass-lifetime relationships from theoretical stellar evolution models, the initial progenitor mass $M_{\rm i}$ is immediately obtained from $t_{\rm prog}$.

It is clear how and where theoretical models play an important role in this procedure. WD cooling models plus progenitor evolutionary tracks and isochrones are needed to determine the various $t_{\rm clus}$, $t_{\rm cool}$ and $t_{\rm prog}$. Given the very short timescale of the AGB evolution (see also next section for a short discussion on this issue) AGB modelling and its related

uncertainties do not play a role in these types of analyses, but uncertainites entering the previous evolutionary phases and the WD cooling stage can affect the derived IFMR. Another important point is the issue of consistency. First of all, the isochrones employed to determine $t_{\rm clus}$ should be computed starting from the same evolutionary tracks adopted to determine $M_{\rm i}$ from the estimated value of $t_{\rm prog}$. Consistency is not usually achieved in existing estimates of the IFMR. Even in the most recent studies of the IFMR, in several cases cluster ages are obtained from earlier studies that have employed models different from the ones used to estimate $M_{\rm i}$. Secondly, all cluster ages should be determined following the same method, and – most importantly – employing the same set of isochrones. Instead, results from different sources for the various clusters are used.

As an example, we summarize briefly the work by Ferrario et al. (2005). The Hyades age has been taken from Perryman et al. (1998), who had calculated their own isochrones with an updated version of the CESAM code (Morel 1997). In case of M35 the age quoted in Table 1 of von Hippel (2005) was employed; this age was derived summarizing the results of three different previous works by other authors. The same is true for the Pleiades, where the assumed cluster age comes from a synthesis of the results of several groups, obtained with different generations of stellar evolution models. The isochrones by Schaller et al. (1992) led Meynet et al. (1993) to an age of 141 Myrs for NGC2516, which was quoted by Ferrario et al. (2005) as 158 Myr. The remaining clusters in that sample also have ages from various isochrone sources, which span more than a decade of progress in stellar evolution modelling, most notably the significant improvements in opacities and the equation of state. The cooling tracks came from Fontaine et al. (2001), and the $t_{\rm prog}$– $M_{\rm i}$ relation from Girardi et al. (2002), taken from the tracks with the metallicity closest to the adopted one, but without interpolation between compositions. It is obvious that there is a certain degree of arbitrariness in the use of stellar evolution theory. This inherent inconsistency is probably the result of the fact that most works on the IFMR are more focused on acquiring new and improved data with an emphasis on the internal errors of their derived $T_{\rm eff}$ and $M_{\rm f}$.

The aim of the present work is instead to concentrate on the stellar evolution models needed for deriving the IFMR. It is obvious from the previous discussion that a consistent use of stellar models and procedures about how to employ them is required, to achieve a higher accuracy. We therefore will make use of calculations of stellar models, that cover all phases from the MS to the WD cooling phase. They will be used for the appropriate metallicity of each cluster, in order to have at hand accurate and homogeneous isochrones and progenitor lifetimes. This will provide an IFMR with the highest internal consistency achieved so far.

To get a measure of the errors introduced by using different codes and input physics,

we also repeat the procedure by using alternative sets of models for the WD cooling and/or progenitor and cluster ages. While this gives a first indication about the size of the systematic errors resulting form different stellar model sources, we finally quantify the influence of various physical effects important for both the isochrone and WD cooling calculations. Using Monte Carlo methods we determine the total extent of the systematic errors. This allows us also to verify which features of the IFMR are robust and which ones depend on present model uncertainties.

Using the robust results, we can finally exclude some of the stellar models because they lead to internal contradictions. One of our conclusions is that models without overshooting from convective cores on the MS do not yield self-consistent results. On the other hand, the parametrization of overshooting during the AGB phase, which influences the growth of the carbon-oxygen core, cannot be the same in all convective layers as it is at the convective core during the MS phase, because it produces final masses inconsistent with observations. We thus can also reduce uncertainties in the physics of stellar interiors.

The structure of the paper is as follows: In Sect. 2 we outline the procedure to obtain an IFMR, summarize the observational input data we have used for the WDs and the parent clusters, and present the set of the stellar models used for determining the reference IFMR as well as for the evaluation of the systematics. Section 3 then concentrates on the estimates of the global error bars, while Sect. 4 contains the results and a comparison with theoretical IFMRs. A summary and conclusions follow in Sect. 5.

2. IFMR determination

As discussed in the Introduction, the method we follow to determine the IFMR makes use of WDs in star clusters. Observations have to provide us with:

- Surface gravity g and effective temperature T_{eff} of individual WDs.

- Observed CMDs, estimates of [Fe/H] and E(B − V) for the clusters harboring the observed WDs.

Theory has to provide:

- Sets of stellar evolutionary tracks, plus isochrones – transformed to the CMD – for a range of age and [Fe/H] values, to determine – in conjuction with theoretical, empirical or semi-empirical distance determination methods – the cluster ages, plus stellar lifetimes.

- WD cooling tracks covering a range of masses, to provide the cooling ages of the observed WDs.

Concerning the cooling tracks, the metallicity of the WD models is irrelevant as the envelopes are of pure H (He and metals have settled below the envelope due to diffusion) and the previous core composition may influence only the chemical profile of the core. This will be investigated in a broader context later in this study.

The method works as already summarized in the Introduction; for each cluster WD with an estimated pair of g and $T_{\rm eff}$ values, linear interpolation within a grid of theoretical WD models provides the mass $M_{\rm f}$ (mainly fixed by the value of g) and the age $t_{\rm cool}$ (mostly determined by the value of $T_{\rm eff}$) of the WD. Isochrone fits to the TO region of the observed $V - (B - V)$ CMD determine the cluster age $t_{\rm clus}$. If the actual cluster [Fe/H] does not correspond to any of the values in the isochrone grid used, we determined the age with the two closest grid values bracketing the cluster [Fe/H]. The final cluster age is then obtained by linear interpolation between these two values.

The difference $t_{\rm clus} - t_{\rm cool}$ represents the lifetime $t_{\rm prog}$ of the WD progenitor, from the MS until the start of the WD cooling. Theoretical mass-lifetime relationships for the cluster metallicity, obtained from the same evolutionary calculations, finally provide the initial progenitor mass $M_{\rm i}$. We employ a quadratic interpolation in mass and a linear interpolation in [Fe/H] among the available model grids to determine $M_{\rm i}$ from the value of $t_{\rm prog}$.

A potential inconsistency in this procedure is the effect of the duration of the AGB thermal pulse phase on the estimate of $M_{\rm i}$. Theoretical models without inclusion of the thermal pulse phase, or predicting an IFMR different from the one obtained semi-empirically, might be providing inconsistent thermal pulse lifetimes, hence wrong values of the total lifetimes, that in turn affect the derivation of $M_{\rm i}$. Luckily, this effect is negligible; estimates of thermal pulse lifetimes obtained from synthetic AGB modelling (Wagenhuber & Groenewegen 1998; Marigo & Girardi 2007) show that the duration of this phase is typically at most within a few Myr (decreasing sharply with increasing total mass) even in extreme cases of the largest possible growth of the CO core. In fact, from full evolutionary stellar models, Serenelli & Fukugita (2007) have shown that the duration of the AGB phase (including both the early-AGB and the thermally pulsating phases), for stars with initial masses between 1 and 8 $M_{\odot}$, is at most 1% of the MS lifetime.

2.1. WD data

Our reference data set comprises 52 WDs in 10 open clusters, plus Sirius B, for a total of 53 DA objects, as reported in Table 1. We considered the same cluster sample as in the recent work by Ferrario et al. (2005), that contains data for WDs in the Pleiades (Ferrario et al. 2005), Hyades and Praesepe (Claver et al. 2001; Dobbie et al. 2004), NGC2516 (Koester & Reimers 1996), NGC3532 (Koester & Reimers 1993), NGC2099 (Kalirai et al. 2005), NGC2168 (Williams et al. 2004; Ferrario et al. 2005). We wish to notice that our Pleiades sample contains only the object listed by Ferrario et al. (2005). We did not include data for additional two WDs (GD 50 and PG 0136+251) discussed by Dobbie et al. (2006b), because their membership of the Pleiades is not absolutely certain.

To this cluster sample we added NGC6819, NGC7789, and NGC1039. For the WDs in the first two clusters, T_{eff} and g values are taken from Kalirai et al. (2008), and from Rubin et al. (2008) for the last one.

The T_{eff}, g and corresponding error estimates for the clusters in common with Ferrario et al. (2005) are the same as in their Table 1, with a few exceptions. Values of T_{eff} and g for two Praesepe WDs (0837+185 and 0837+218), identified as WD #13 and #14 in Table 1, have been updated following Dobbie et al. (2006a). The same authors provide data for four additional WDs in the same cluster (ID numbers from 16 to 19 in Table 1), that we have included in our analysis. And finally, we also use their data for the single Pleiades WD.

As an additional note about the cluster WD sample, our referee (K. Williams) has pointed out that the Hyades WD 0437+138, that appears as WD #8 in Table 1, has been incorrectly included as a DA object in (Ferrario et al. 2005) study. In fact, it is a DBA WD, with $\log(n_H/n_{He})=-4.5$ in the atmosphere. To assess the errors in the derived mass and cooling age for this object when using DA models, we have made the following test. We have compared $\log(g)$ values derived from DB and DA models at the observed T_{eff} of WD #8, for the two extreme cases of 0.55 and 1.0 $M_{\odot}$ (the mass we obtain from the analysis with DA models is $\sim 0.77 M_{\odot}$). Our adopted DB models have been computed as described in Salaris et al. (2001).

For both masses the difference in $\log(g)$ derived from the DA and DB tracks is smaller than the 1σ error bar on the observed value for WD #8 (as listed in Table 1). Also the difference in cooling ages at the observed T_{eff} is well below the error bars we derive from our analysis, as reported in Table 5. This implies that the analysis of WD #8 with DB models would provide mass and cooling age compatible (within the 1σ errors) with the results obtained from the DA models employed in this analysis. The reason is that the mass-radius relation is not strongly affected by the atmospheric composition, and also at

the relatively high T_{eff} of this object the evolutionary timescales of DA and DB models are similar. Moreover, given that this WD does not have a pure-He envelope, differences will be even more negligible.

In addition to a large sample of cluster WDs, we also include Sirius B in our analysis. The data for Sirius B (also included in Ferrario et al. 2005) in Table 1 are from the recent determination by Barstow et al. (2005). From the estimated mass and radius of the primary MS star (Sirius A) one can derive its age by comparison with stellar evolutionary tracks in the mass-radius plane. We assumed [Fe/H]=0.0 for Sirius A, following Liebert et al. (2005), to which we associated an 0.10 dex 1σ error. The age of the star is obtained from models bracketing the metallicity of the system (if different from the values provided by the employed isochrone grid). Linear interpolation in [Fe/H] between the two bracketing results gives then the age for the appropriate [Fe/H]. The age of Sirus A provides the age of the system t_{sys}. Sirius B cooling time t_{cool} and mass are determined from the spectroscopic T_{eff} and g estimates, as described before. The difference t_{sys}-t_{cool} provides the age of the Sirius B progenitor, hence M_{i} after using a grid of theoretical lifetimes for solar metallicity.

2.2. Cluster data

The sources for the cluster [Fe/H], E(B-V), and their CMDs used for age determinations, are listed in Table 2.

Values for [Fe/H] have been taken mainly from the compilation by Gratton (2000), who presents a collection of [Fe/H] estimates for a large sample of open clusters, recalibrated against results from high-resolution spectroscopy. Alternative estimates have been adopted for NGC2099, which is not in the Gratton (2000) compilation, NGC6819 and NGC1039, for which recent high-resolution spectroscopic measurements have appeared in the literature (see Table 2).

Reddenings are taken from the compilation by Loktin et al. (2001). These are weighted averages of estimates obtained with various methods, all based essentially on color-color relationships. For NGC6819 we employed a very recent E(B-V) determination based on spectroscopy (Bragaglia et al. 2001), and for the Pleiades reddenings to individual stars have been adopted, as discussed in Percival et al. (2003). The case of NGC7789 is discussed below.

In case of Hyades and Praesepe we have assumed – as usual – zero reddening. Throughout this paper we use $A_{\mathrm{V}} = 3.2\, E(B-V)$. We adopted a 0.02 mag uncertainty in $E(B-V)$ when no error is quoted by the source of the data.

To estimate the age of the whole cluster sample we have followed a two-step procedure where we tried to minimize the inputs from theoretical isochrones. First, cluster distance moduli have been determined using a fully empirical MS-fitting to the $V - (B - V)$ CMDs, that makes use of the sample of field dwarf with accurate $Hipparcos$ parallaxes and [Fe/H] presented by Percival et al. (2003). Details about the method can be found in the same paper.

Here we just recall that for each cluster a MS fiducial line has been derived, by plotting color histograms in V-magnitude bins, and considering the mode of the resulting distribution. In this way one minimizes the impact of unresolved binaries. The resultant points are fitted to a cubic function that provides the cluster fiducial line. After applying (empirical) color corrections that account for the actual cluster metallicity and for the reddening E(B-V), the field dwarf template sequence is shifted in magnitude to match the MS fiducial line, and the apparent distance modulus is obtained by χ^2 minimization. For objects like NGC2168 or the Pleiades, with an extremely well defined and thin (in color) MS, the separation of the binary sequence is very evident, and a cubic fit directly to the single star MS is performed in order to derive the fiducial line.

In case of NGC3532 we could not find available data with good photometry in the MS magnitude range of our template field dwarf sample. The distance modulus of this cluster has been obtained by comparison with Praesepe, that has the same [Fe/H] within errors (and also a comparable age). The larger (as compared to our other estimates) error bar on its distance (hence on its age) reflects this less direct determination of the distance modulus.

As a final remark, we wish to notice that, as discussed i.e. in Percival et al. (2003), a simultaneous MS-fitting to both VI and BV data can provide both the cluster distance modulus and reddening. This procedure has been applied (using the same field dwarf sample, that has homogeneous BVI photometry) to NGC7789, employing additionally the VI data by Gim et al. (1998). Our adopted E(B-V) for NGC7789, used also in Percival & Salaris (2003), has been determined in this way. This method to determine the reddening could not however be applied to the whole cluster sample because of the lack of suitable BV and VI photometry for all clusters.

For a few clusters we have used distances already published in the literature, obtained with the same technique and the same $Hipparcos$ field dwarf sample. More in detail, for the Hyades we have used the result by Percival et al. (2003), that is in perfect agreement with the $Hipparcos$ distance by Perryman et al. (1998). For the Pleiades we have used the distance modulus determined by Percival et al. (2005), while for NGC7789 we have employed the result by Percival & Salaris (2003). The cluster NGC6791, which is also part of the investigation by Kalirai et al. (2008) was not considered in our analysis because its

metallicity [Fe/H]∼+0.45 (Gratton et al. 2006) is higher than the upper [Fe/H] range of the field dwarf sample ([Fe/H]=+0.30), and therefore we could not apply this empirical method to determine its distance. Since we did not want to introduce a second, inconsistent method, we disregarded this cluster.

Second, isochrone fits to the TO region (in the $V - (B - V)$ plane), employing the distance moduli derived in the previous step, determine the cluster age.

The final ages for various choices of the isochrone grid, as well as the adopted cluster [Fe/H] and $E(B - V)$ values are reported in Table 3. Age uncertainties are due to both distance (which is in turn affected by the assumed [Fe/H] and $E(B - V)$ values and their errors) and [Fe/H] uncertainties. Figure 1 compares the ages obtained with the BaSTI overshooting isochrones (that throughout the paper will be considered as our reference set of models to determine the IFMR; see Sect. 2.3) with the ages adopted by Ferrario et al. (2005) for the clusters in common (plus Sirius A). In spite of the dishomogeneity in terms of methods, data and isochrones employed, the two sets of ages compare well, within the respective error bars. The only exception occurs for NGC2099 (M37), for which our derived distance modulus is 0.4 magnitudes larger than implicitly assumed in Ferrario et al. (2005) – who adopt the age estimate by Kalirai et al. (2001b) – leading to a smaller cluster age (320 Myr as compared to 520 Myr). However, if we adopt a lower metallicity and reddening as suggested by Kalirai et al. (2005) and discussed in Sect. 2.4 (see Table 3) we derive an age of 550 Myr for NGC2099, in close agreement with Ferrario et al. (2005). Obviously, at this time the uncertainties in the cluster parameters dominate the determination over those from using different theoretical isochrones, which constitutes our first result.

2.3. Models

Our reference IFMR is defined by the use of the following set of models. We refer the reader to the original papers quoted below for details of the models and calculations.

– Pietrinferni et al. (2004) models from the MS to the AGB with the inclusion of core overshooting during the central H-burning phase (hereafter BaSTI models with overshooting), to estimate in a consistent way both $t_{\rm clus}$ and $t_{\rm prog}$.

– Salaris et al. (2000) WD cooling models (hereafter S00 WD models) to estimate $t_{\rm cool}$. The code employed to compute these WD models is the same as for the progenitors. Some major sources of input physics in the WD models (see S00) are different from what has been employed in BaSTI models, most notably equation of state and low-temperature opacities. This is somewhat unavoidable, given the different range covered by many physical parameters

throughout WD structures, as compared to their progenitors. It is very important to remark here about the internal CO stratification of the WD models. The CO profile in the inner core of a WD is built up during the central He-burning phase, whereas the more external part of the WD core is processed during the early AGB phase and the thermal pulses. Current uncertainties in the treatment of mixing in stellar interiors and in some key reaction rate (i.e., the $C^{12} + \alpha$ reaction) introduce additional uncertainties in the predicted CO profiles. S00 models employ a CO stratification obtained from evolutionary models of solar metallicity progenitors, from the MS until the completion of the first thermal pulse (Salaris et al. 1997). The core mass and associated CO profile at the end of the pulse were taken as representative of the final WD object. When estimating the total error budget in the IFMR, we have accounted for the uncertainties in the CO profiles by using WD models with different C/O mass fraction ratios in their cores. This will be described in detail in Sect. 3. We anticipate, however, that these uncertainties are very small since all the WD stars in our sample have not entered yet the crystallization phase, where the detailed core composition could have a larger effect.

We have studied systematic effects on the IFMR relation due to:

i) Different model grids. We redetermine the IFMR employing Girardi et al. (2000) models from the MS to the AGB (hereafter Padua models; they also include core overshooting but with a different formalism compared to BaSTI), keeping the WD models unchanged (S00).

ii) Effect of overshooting. We redetermine the IFMR employing Pietrinferni et al. (2004) models from the MS to the AGB without core overshooting (hereafter BaSTI no-OV models), again keeping the WD models unchanged (S00).

iii) Different WD model grids. We redetermine the IFMR employing the WD models computed with the LPCODE (hereafter LPCODE models; details of the LPCODE are given in Althaus et al. 2003), keeping the progenitor models unchanged (BaSTI with overshooting). This tests not only different codes, but also – in an unsystematic way – variations of the physics employed and of the WD chemical stratification.

iv) Systematic variation in WD input physics and chemical profiles. We redetermine the IFMR employing the LPCODE WD models, by varying the CO-core stratification, H-envelope thickness, electron conduction opacities and neutrino energy loss rates. In this case, the progenitor models are unchanged throughout (BaSTI with overshooting).

2.4.   The reference IFMR

We present in this section our reference IFMR, while we defer to subsequent sections the discussion of the uncertainties involved in the IFMR determination. We use the S00 WD models to derive the WD (final) masses and cooling ages. Using our reference cluster ages (fifth column in Table 3) and the BaSTI models with overshooting we construct the IFMR by deriving the progenitor (initial) masses. Figure 2 displays this reference semi-empirical IFMR. Error bars include all uncertainty sources we consider. We defer a detailed discussion to Sections 3 and 4, but note here that the most relevant sources of uncertainty are due to the following effects: (i) errors in the WD T_{eff} and g values; (ii) uncertainties in the cluster [Fe/H]; these affect the age through their influence on the derived cluster distance (mainly) and on the isochrones to be used for the age determination; (iii) errors in the reddening $E(B - V)$, which influence the age determination through the effect on the cluster distance. In case of one star (WD #38 in NGC2099) the progenitor age results to be negative. We did not consider this object in the analysis of the IFMR.

We have performed at this stage a simple check of our reference IFMR, comparing the distribution of M_{i} and M_{f} values with Ferrario et al. (2005) – disregarding the attached error bars – by means of a bi-dimensional Kolmogorov-Smirnov (KS) test (Press et al. 1992). We considered only clusters (plus Sirius) in common between the two studies. As customary, we accept the existence of a significant difference between the two IFMRs if the probability P that the two samples of (M_{i}, M_{f}) pairs were drawn from different distributions was higher than 95%. We obtain P values smaller than 50%, highlighting the statistical agreement between our reference IFMR and Ferrario et al. (2005) results for the clusters (plus Sirius B) in common.

We have also performed analytical fits to the data. In doing this, we have left out the data from NGC2099 because our results for this cluster show some anomalies, e.g. a progenitor with negative age (WD #38 mentioned above), a 0.45 $M_{\odot}$ WD with a progenitor mass above 8 $M_{\odot}$ (WD #37) and some other issues to be discussed later in the paper.

In Figure 2 we show two analytic fits to the data. The first one, linear, gives

$$M_{\mathrm{f}} = 0.084 M_{\mathrm{i}} + 0.466 \tag{1}$$

and a reduced chi-squared $\chi_r^2 = 3.7$. Approximate values for the 1σ rms dispersion about this relation are: 0.075 $M_{\odot}$ below 2 $M_{\odot}$, 0.12 $M_{\odot}$ between 2.7 and 4 $M_{\odot}$, 0.09 $M_{\odot}$ between 4 and 6 $M_{\odot}$ and then it increases almost linearly up to 0.20 $M_{\odot}$ at around 8.5 $M_{\odot}$.

Guided by theoretical models, which show a break in the slope of the IFMR at around 4 $M_{\odot}$ (see Fig. 3), we have also performed a piecewise linear fit with a pivot point at

$M_i = 4$ M$_\odot$ that yields

$$M_f = \begin{cases} 0.134M_i + 0.331 & 1.7 \text{ M}_\odot \leq M_i \leq 4 \text{ M}_\odot \\ 0.047M_i + 0.679 & 4 \text{ M}_\odot \leq M_i. \end{cases} \tag{2}$$

This fit gives $\chi_r^2 = 2.7$ at the expense of introducing only one more free parameter (we force the fit to be continuous at the pivot point). In this case, the dispersion is reduced to 0.05 M$_\odot$ below 2 M$_\odot$ and to 0.09 M$_\odot$ above 6 M$_\odot$, while it remains basically unchanged anywhere else. The reader should keep in mind that these cluster data do not constrain the IFMR at masses lower than about 1.7 M$_\odot$. As a consequence, the present analytic relations, particularly the piecewise linear fit, should not be extrapolated towards lower initial masses.

We could attempt more complicated fits to the data, but in our opinion the uncertainties in mass determinations, and possibly the existence of an intrinsic spread in the IFMR to be discussed below, render such efforts probably unnecessary. In fact, we have found polynomial fits beyond second order do not produce any relevant improvement in the goodness of fit.

As an additional check, we performed a direct comparison of our fits with the polynomial relationship from Ferrario et al. (2005), that was derived by combining an assumed star formation rate and initial mass function for the Galactic Disk, with the observed field WD mass distribution. For masses between 2.5 and 6.5 M$_\odot$ – the range of initial masses covered in their study – at a given M_i, differences in the M_f values are less than 0.04 M$_\odot$, well below the dispersions given above.

Another point that we wish to address is the presence of a possible intrinsic spread in the reference IFMR, as noticed by Reid (1996) in an analysis of Praesepe WD population. With intrinsic spread we mean a signature of differential mass loss among stars with the same mass and same initial chemical composition. Catalán et al. (2008a) have investigated very recently the spread around their mean semi-empirical IFMR (determined from cluster WDs and WDs in common proper motion pairs) and found no clear cut indication that is either due to a spread in mass loss or to some other individual stellar properties (e.g. the thickness of the envelope layers) that vary between objects.

To investigate this issue with our data, we made the following test. We considered objects in a single cluster, namely Praesepe, with M_i values in agreement within their respective 1σ error bars. There are 8 stars with M_i between 3.045 and 3.543 $M_\odot$ satisfying this constraint, and we assume that – within the present error bars – they share the same M_i, equal to the average value $\langle M_i \rangle = 3.207$ $M_\odot$. For these objects, the average WD mass is $\langle M_f \rangle = 0.769$ $M_\odot$ with 1σ rms equal to $0.045M_\odot$. To test whether this observed dispersion in M_f is due exclusively to the errors in the M_f estimates, we built a synthetic sample by drawing randomly 10000 M_f values for each of the 8 objects, according to a Gaussian

distribution centred on $\langle M_f \rangle = 0.769\ M_\odot$, with a 1σ spread given by their individual error bars. The synthetic distribution has obviously $\langle M_f \rangle = 0.769\ M_\odot$, but a 1σ rms equal only to $0.028 M_\odot$. We compared statistically the σ values of the two distributions by means of an F-test, that returned a probability of $P=96.3\%$ that σ of the synthetic sample is different from (smaller than) the observed one. By fixing, as customary, a threshold of $P=95\%$ to accept the existence of a real difference between the two σ values, our simple test seems to point to the existence of a spread in the IFMR, at least in this cluster. Adding 5 more objects in the Hyades and in NGC3532 (the [Fe/H] estimates for these two clusters plus Praesepe span a range of only $\sim$0.10 dex, and overlap within their associated $\sim 2\sigma$ error bars, see Table 3) with initial masses within the same overlapping M_i range and repeating the previous analysis does not change this conclusion. In fact, for this enlarged sample, $\langle M_f \rangle = 0.729\ M_\odot$, with a 1σ rms equal to $0.10 M_\odot$. The probability that the corresponding synthetic sample – constructed in the same way as for the 8 Hyades WDs – has a different σ than observed is $P=96.9\%$.

However, this evidence for an intrinsic spread (i.e. due to a significantly varying mass loss at a fixed mass and chemical composition) in the IFMR is weakened if we take into account theoretical expectations for near-solar metallicities, displayed in Fig. 3. Although the M_i values estimated for these 13 WDs (or just the 8 Praesepe objects discussed above) overlap within the 1σ error bars, the same error bars suggest that they may also cover a range of values. Just considering the range covered by the central M_i estimates for these 13 WDs, theoretical IFMRs (see also another completely independent theoretical IFMR for solar metallicity in Fig. 3 of Prada Moroni & Straniero 2007) generally display a steep rise of M_f with M_i. Over the M_i range between 3.05 and 3.5 $M_\odot$, the theoretical IFMRs of Fig. 3 predict an increase in M_f by about 0.1 $M_\odot$, which corresponds to $\sim 2\sigma$ of the observed M_f spread in the 8 Praesepe objects, and to $\sim 1\sigma$ of the observed spread in the 13-object enlarged sample. Without accounting for errors in the estimate of M_f, the predicted change within the M_i range allowed by the error bars of the estimated initial masses can potentially explain the observed M_f spread. This would imply that the observed spread is not the result of star-to-star mass loss variations, but due to, as predicted from theory, the steep increase of M_f with M_i in the relevant mass range.

Moving this analysis to different M_i ranges can hardly provide additional constraints on the existence of an intrinsic spread in the IFMR, because of either smaller numbers of objects in comparable M_i intervals (when moving to lower M_i values) or a combination of much larger error bars on M_i and small numbers (when moving to higher M_i values). It may however be interesting to notice the situation at $M_i \sim 1.8\ M_\odot$, where we have 5 objects (belonging to NGC7789 and NGC6819) with formally the same M_i, small errors in both M_i and M_f and theoretical predictions for an IFMR essentially flat (see Fig. 3). By applying the

same statistical analysis described before we do not find any statistically significant spread in the IFMR for this sample.

Before concluding this section we discuss briefly another test of our reference IFMR. In the case of NGC2099 we have considered the alternative value [Fe/H]=−0.20 and reduced reddening (E(B-V)=0.23) used by Kalirai et al. (2005) and given by Deliyannis et al. (2002). Note however that Deliyannis (private communication) considers this as a possible but as yet unconfirmed value for [Fe/H]. Using this alternative metallicity and reddening we derive an age for NGC2099 of 550 Myr which, compared to 320 Myr derived with [Fe/H]=0.09, has a dramatic effect in the inferred initial masses (Fig. 7). Results for NGC2099 stars (#27-#38) are repeated in the last part of Table 6 but in this case corresponding to the low [Fe/H]. As expected from the relatively large change in the inferred cluster age, changes in M_i due to the different cluster parameters generally exceed the uncertainties in M_i determination.

This test, based on estimates that are admittedly not confirmed, is just to exemplify in a quantitative way how crucial the assessment of the cluster [Fe/H] and E(B-V) values is.

We will return to this issue in Sect. 4.

3. Global error-bar estimates

The method used to determine the IFMR has been described in Section 2, where we also presented our reference IFMR. We now focus on a detailed determination of the global uncertainties both in the initial and final masses for each star in our sample. Since the global errors have contributions from various sources, they have been estimated by means of Monte Carlo simulations. In the following we detail the procedure followed for each star in our sample.

3.1. White Dwarf Uncertainties

We have tried to cover all major sources of uncertainties in the WD mass and cooling age determinations, that are going to be discussed in this section. While we have used S00 models as our standard set of WD models, all the WD evolutionary sequences to test the effect of WD input physics and chemical stratification have been computed with the LPCODE described below. This should not invalidate our procedure, since we are using LPCODE models only to determine differential changes in the WD properties (e.g. core composition), not absolute values. In what follows, X represents the logarithmic values of either the WD mass or the cooling age.

– Observational uncertainties. The central values and 1σ uncertainties for $\log g$ and T_{eff} are listed in Table 1. We leave them unmodified as they are given in the original papers quoted in Sect. 2.1.

– Systematic uncertainties from WD cooling tracks. In addition to our standard choice of WD cooling tracks (S00), we have specifically computed a completely independent set of WD cooling models with the LPCODE. The aim is to estimate the *systematic* uncertainties in the inferred WD properties that arises from using different WD models. We define the 1σ uncertainty by

$$\sigma_{\mathrm{syst}}(X) = |X_{\mathrm{S00}} - X_{\mathrm{LP}}|; \tag{3}$$

where X_{S00} is derived from S00 models and X_{LP} from models computed with the LPCODE. WD models computed with the LPCODE have been used in Serenelli & Fukugita (2007), where the evolution of a set of stellar models from 1 to 8 $M_{\odot}$ and solar metallicity has been consistently followed from the main sequence phase up to the WD phase, including the thermal pulse (TP) AGB phase. It should be noted that, in addition to differences in numerics, $\sigma_{\mathrm{syst}}(X)$ also accounts for differences in input physics between the two sets of models. While S00 and LPCODE models have used the same neutrino energy loss rates (Itoh et al. 1996), conductive opacities in the CO cores (Itoh et al. 1993) and very similar hydrogen envelope thickness and core composition, they differ in other relevant aspects such as the equation of state and low temperature opacities (see Althaus et al. 2003 and Salaris et al. 2000 for details about the LPCODE and S00 input physics respectively) and the inclusion of gravitational settling in the model envelopes (S00 models mimic the effects of gravitational settling by adopting a pure hydrogen envelope and fixed chemical H/He and He/C/O interfaces while in LPCODE the chemical profiles are evolved according to time-dependent equations of element diffusion).

– Neutrino energy loss rates. For the WD evolutionary sequences we are considering in this work, plasma neutrinos always contribute at least 90% of the total neutrino emission. Uncertainties in the theoretical calculation of plasma neutrino emission rates, within the framework of the standard model of particle physics, are at most a few percent (Fukugita, private communication) and thus we do not expect them to represent an important source of uncertainty in determining WD cooling ages. Several additional cooling mechanisms that could operate in WD interiors have been proposed, e.g. enhanced neutrino cooling due to a non-null neutrino magnetic dipole moment, axion production or other particles like Weakly Interacting Massive Particles (see Raffelt 1996 for a complete discussion of these mechanisms). It is not our aim here to consider the effects on the WD properties – particularly on the cooling rate – of all such mechanisms, especially because they remain

purely hypothetical[1]. We do not want, however, ignore the possibility that some additional cooling might be present. Consequently, we have adopted a more conservative point of view and have computed additional WD cooling models where standard neutrino energy loss rates (Haft et al. 1994; Itoh et al. 1996) have been multiplied by factors of 2 and 0.5 respectively to take into account the possibility of such additional cooling mechanisms. These large factors were chosen to represent our conservative approach. We define the WD mass (and cooling age) 1σ uncertainties due to neutrino energy losses as

$$\sigma_\nu(X) = \frac{|X_2 - X_{0.5}|}{2}, \tag{4}$$

where the subindices refer to quantities corresponding to the WD cooling models with the modified neutrino emission rates as described above.

– Conductive opacity. For the physical conditions and composition of a representative set of WD models, we have computed conductive opacities according to both Itoh and collaborators (Itoh et al. (1993) and references therein – our references set of conductive opacities) and Potekhin and collaborators (see Cassisi et al. 2007 for the most up to date calculations). We find differences between both sets of calculations to be usually below 20% for the range of temperatures and densities relevant to the WD models used in this paper. In analogy with the neutrino emission rates, we have estimated the effect of electron conduction uncertainties by computing additional WD models where the conductive opacities from Itoh and collaborators have been multiplied by factors of 1.25 and 0.8 and have used these models to define the WD mass and cooling age 1σ uncertainties due to errors in conductive opacities calculations as

$$\sigma_\kappa(X) = \frac{|X_{1.25} - X_{0.8}|}{2}. \tag{5}$$

– WD core composition. The mass fraction of the central oxygen X_O in S00 WD models ranges from 0.65 up to 0.80 depending on the mass of the WD. The internal CO stratification is however subject to uncertainties due to the uncertainty on the $C^{12} + \alpha$ reaction rate (see, e.g. S00) and, very important, the treatment of mixing (semiconvection, breathing pulses and the mechanism to suppress them) during the central He-burning phase (Straniero et al.

---

[1]Among the non-standard cooling mechanisms, axions are probably the best motivated. Recently, Bischoff-Kim et al. (2008) and Isern et al. (2008) have used WD pulsation properties and the luminosity function of local Disk WDs, respectively, to constrain the axion mass m_a. While Bischoff-Kim et al. (2008) find an upper limit $m_a = 13$ meV, Isern et al. (2008) rule out values as low as 10 meV and give a preferred value of $m_a = 5$ meV. With this mass value, axion cooling is never the dominating WD cooling mechanism (contrary to neutrino cooling, that dominates for hot WDs) but it is strong enough that it can have a moderate effect on WD age determinations for WDs with luminosities in the range $-1.2 < \log L/L_\odot \lesssim -1.7$.

2003). These effects are larger than the expected change in CO profiles due to the small metallicity range covered by the cluster sample. In our analysis we have been conservative and have defined the 1σ uncertainty due uncertainties in the core composition as

$$\sigma_{\text{core}}(X) = \frac{|X_{0.9} - X_{0.3}|}{2}, \tag{6}$$

where $X_{0.9}$ and $X_{0.3}$ are derived from WD cooling tracks where the original chemical profiles have been rescaled to have $X_{\text{O}} = 0.9$ and 0.3 at the center, respectively.

   – Hydrogen envelope thickness (M_{H}). As shown by, e.g., Provencal et al. (1998) the H-envelope thickness of DA WDs displays a range of values. To include this effect in our error analysis, in addition to the standard thick envelopes considered in our LPCODE calculations (usually 10^{-4} $M_{\odot}$, but larger values were used for WD masses below 0.6 $M_{\odot}$) we have computed also cooling sequences with thinner H-layers of 10^{-6} $M_{\odot}$. Similar to the above procedures, we have defined the corresponding 1σ errors

$$\sigma_{\text{env}}(X) = \frac{|X_{\text{thick}} - X_{\text{thin}}|}{2}; \tag{7}$$

where X_{thick} and X_{thin} are derived from WD models with thick and thin hydrogen envelopes respectively. We have performed an additional test to explore very thin hydrogen envelopes (as in Catalán et al. 2008a) by computing a 0.6 and a 1 $M_{\odot}$ WD models with hydrogen envelopes of $M_{\text{H}} \sim 10^{-10}$ $M_{\odot}$. When compared to models with thick envelopes, we have found that differences in the cooling ages never exceeded 11% in both cases and are usually at the level of 7% for the 0.60 $M_{\odot}$ model and 5% for the more massive one in the range of effective temperatures of interest to this work. Asteroseismology studies of ZZ Ceti stars disclose a wide range of hydrogen envelope thickness, ranging between $\sim 10^{-4}$ $M_{\odot}$ and $\sim 10^{-9}$ $M_{\odot}$ (see, e.g., Castanheira & Kepler 2008). In this regard, the changes in the cooling ages due to uncertainties in the H-envelope thickness quoted above can probably be taken as robust upper limits.

   For neutrino emission rates, conductive opacities, core composition and hydrogen-envelope thickness we have assumed that uncertainties distribute normally. In the case of systematic uncertainties from different WD cooling tracks we have assumed uniform distributions of uncertainties (f_X) which are defined, in each case, by $\int_{-\sigma_{\text{syst}}}^{+\sigma_{\text{syst}}} f_X dX = 0.683$. We tabulate $\sigma_{\nu}(X)$, $\sigma_{\kappa}(X)$, $\sigma_{\text{core}}(X)$, $\sigma_{\text{env}}(X)$ and $\sigma_{\text{syst}}(X)$ in ($\log g$, T_{eff}) grids for using them in the Monte Carlo simulations. We summarize the results for the WD uncertainties, both for mass and cooling age, in Table 4, where for a small subset of ($\log g$, T_{eff}) values, we give the $1 - \sigma$ fractional uncertainties in WD mass and cooling age as defined by Eqs. 3-7, but transformed to linear scale to facilitate interpretation of the results.

3.2. Progenitor Star Uncertainties

Progenitor masses M_i are obtained from the estimated progenitor lifetime and stellar models. In addition to the uncertainty sources discussed in the previous section for t_cool, the determination of M_i is affected by:

– Cluster age. Progenitor lifetimes are obtained simply as $t_\mathrm{prog} = t_\mathrm{clus} - t_\mathrm{cool}$, so uncertainties in t_clus directly affect the determination of M_i. Central values and adopted 1σ uncertainties for the cluster ages determined for this paper are listed in Table 3. As our standard choice, we have adopted uniform distributions $f_t(t_\mathrm{clus})$ for cluster age uncertainties, where f_t is a constant defined by the simple relation $\int_{-\sigma_{t\mathrm{clus}}}^{+\sigma_{t\mathrm{clus}}} f_t \, dt_\mathrm{clus} = 0.683$.

– Stellar metallicity ($\Delta[\mathrm{Fe/H}]$). $\Delta[\mathrm{Fe/H}]$ affects the determination of M_i in two different ways. The first and most important relates to the determination of the cluster age (mainly through the change in the distance modulus obtained via MS-fitting) and has already been taken into account in the uncertainty of t_clus. Additionally, $\Delta[\mathrm{Fe/H}]$ introduces uncertainty in the determination of the progenitor mass because, for different metallicities, a fixed t_prog corresponds to different progenitor masses. We treat this effect by adopting the central values and uncertainties in the metallicities listed in Table 3 to generate stellar metallicity distributions (normal distributions are our standard choice). For a fixed t_prog we then compute M_i for the corresponding metallicity distribution.

– Different stellar models and isochrones. In order to estimate the systematic uncertainties arising from using different sets of stellar models and isochrones we have proceeded in a similar fashion as in the case of the WD cooling tracks and define as the 1σ uncertainty

$$\sigma_\mathrm{syst}(M_\mathrm{i}) = |M_\mathrm{i,BaSTI} - M_\mathrm{i,Padua}|; \tag{8}$$

where $M_\mathrm{i,BaSTI}$ represents the progenitor masses derived with Basti stellar models and isochrones and $M_\mathrm{i,Padua}$ those derived with Padua models and isochrones. We have adopted a uniform distribution for systematic uncertainties. It should be noted here again that consistency in the calculations requires the same set of models and isochrones be used to derive M_i and t_prog, i.e. the cluster age. It is in principle not correct to adopt a cluster age derived with, let us say the BaSTI isochrones, and then the Padua stellar models to derive M_i from the calculated t_prog. As already stated in the Introduction, such inconsistencies are ubiquitous in the current literature and can introduce noticeable systematic changes in the derived M_i, particularly for $M_\mathrm{i} \gtrsim 5\mathrm{M}_\odot$.

We close this section by stressing that both codes, BaSTI and Padua, are employing up-to-date physics input, and therefore are, at least nominally, quite similar in their treatment of stellar evolution. Systematic uncertainties arising from code-to-code differences are therefore

possibly underestimated in the above error analysis, if they arise from different physical assumptions, as, for example, the inclusion or neglect of convective overshooting, which we did not include in the discussion of this section (we provide separate results for models without core overshooting).

When considering models without core overshooting, the systematic effect of using different models and isochrones was taken into account with a slightly different approach because Padua calculations are only available for one chemical composition, i.e. $Z{=}0.019$ and $Y{=}0.273$. This pair of (Y, Z) values corresponds to [Fe/H]=0.04 when considering the Grevesse & Noels (1993) solar mixture (that provides $Z/X{=}0.0245{\pm}0.005$ for the present Sun) employed in those stellar model calculations. Also BaSTI models employ the Grevesse & Noels (1993) solar mixture, and the (Y, Z) pair closest to the Padua one around the solar metallicity is $Z{=}0.0198$, $Y{=}0.2734$, that corresponds to [Fe/H]=0.06. In this case, and just for estimating this systematic uncertainty, we have computed all progenitor masses for both BaSTI and Padua non-overshooting models assuming a fixed [Fe/H]=0.04 for Padua and [Fe/H]=0.06 for BaSTI. As above, the difference between the masses has been adopted as a measure of the systematic uncertainty and we have assumed this difference does not depend on the actual [Fe/H] value. This is in fact a reasonable approximation and, in addition, systematic uncertainties from isochrones and models turn out to be a small contribution to the overall uncertainty budget, so our simplified treatment should not affect our results and conclusions.

3.3. Monte Carlo simulations

For each star in our sample, the Monte Carlo (MC) simulations consist of the following steps:

– generate $\{\log g_{\mathrm{j}}, T_{\mathrm{eff,j}}\}_{\mathrm{j=1}}^{\mathrm{N}}$ distributions according to observational uncertainties and use S00 WD models to get the initial WD mass $\{M_{\mathrm{f,j}}^0\}_{\mathrm{j=1}}^{\mathrm{N}}$ and cooling age $\{t_{\mathrm{cool,j}}^0\}_{\mathrm{j=1}}^{\mathrm{N}}$ distributions. Here $N({=}\,10^5)$ is the total number of trials in the MC simulations and quantities with the j suffix denote results of each one of the trials;

– For each trial j include additional WD mass and cooling age uncertainties according to the details given in Section 3.1. Each mass in the the final WD mass distribution $\{M_{\mathrm{f,j}}\}_{\mathrm{j=1}}^{\mathrm{N}}$ (analogously for the WD cooling age) is given by

$$M_{\mathrm{f,j}} = M_{\mathrm{f,j}}^0 + \sum_{\mathrm{k=1,5}} \delta M_{\mathrm{j,k}}, \tag{9}$$

where each $\delta M_{\mathrm{j,k}}$, the individual contributions to the WD mass global uncertainty, is ran-

domly drawn from distributions constructed as described in Section 3.1. The final WD cooling age distribution $\{t_{\mathrm{cool,j}}\}_{j=1}^{N}$ is computed in the same way;

– generate the cluster age distribution $\{t_{\mathrm{clus,j}}\}_{j=1}^{N}$ and then the progenitor age distribution $\{t_{\mathrm{prog,j}}\}_{j=1}^{N}$, where for each trial $t_{\mathrm{prog,j}} = t_{\mathrm{clus,j}} - t_{\mathrm{cool,j}}$;

– From $\{t_{\mathrm{prog,j}}\}_{j=1}^{N}$ get the initial progenitor mass distribution $\{M_{\mathrm{i,j}}^{0}\}_{j=1}^{N}$ using the BaSTI stellar models;

– The final progenitor mass distribution $\{M_{\mathrm{i,j}}\}_{j=1}^{N}$ is obtained by adding the star metallicity and stellar models systematic uncertainties, i.e. $M_{\mathrm{i,j}} = M_{\mathrm{i,j}}^{0} + \delta M_{\mathrm{i,[Fe/H]}} + \delta M_{\mathrm{i,syst}}$ as discussed in Section 3.2.

4. Results and comparisons with theory

4.1. Global error assessment

Table 5 displays the results about cooling age and mass for all the WDs in our sample. The central values have been obtained using S00 WD models and the uncertainties are the result of the MC simulations described in the previous section and thus include *all sources of uncertainty considered in this work*. We also provide, as additional information, the bolometric luminosity of the WDs, as obtained from the interpolation among the WD model grid in $\log g$ and T_{eff}. It is important to notice that none of the objects have yet entered the crystallization phase. This minimizes the effect of uncertainties in the interior CO profiles, that play a very important role during the phase separation associated to the crystallization process (S00).

Our reference IFMR relation (BaSTI with core overshooting plus S00 models) is displayed in Table 6 (labelled "ov"). For the WD masses, the quoted uncertainties are the average of $\sigma_{-}(M_{\mathrm{f}})$ and $\sigma_{+}(M_{\mathrm{f}})$ given in Table 5. For the progenitor masses we give the results of our Monte Carlo simulations, that show strongly asymmetric error bars arising from the highly non-linear relation between evolutionary lifetime and mass for MS stars. Results for BaSTI models without core overshooting are also shown (labelled "non-ov").

As already discussed, our estimates of the global uncertainties in the IFMR include systematic effects due to the use of different sets of stellar models and isochrones, and different WD cooling models. It is instructive, however, to try to single out the influence of the stellar models on the final error. To this aim, Fig. 4 shows a comparison between the progenitor masses obtained with two different sets of stellar models and isochrones (BaSTI and Padua). In both cases we used S00 WD models. When compared with the error bars

on M_i shown in Fig. 3, Fig. 4 leads us to conclude that systematic uncertainties from using different sets of isochrones and stellar models do not contribute appreciably to the global error budget on M_i, as long as the assumptions concerning the stellar physics are similar. We emphasize again that to achieve internal consistency the same set of isochrones and stellar models must be used to determine the cluster ages and to obtain progenitor masses from the progenitor lifetimes.

We next study the changes in the IFMR from using different WD models. Figure 5 displays our reference IFMR (S00 + BaSTI with overshooting) and that resulting from using the LPCODE WD models. Although WD masses derived from both sets of WD models are very similar, the effect on the progenitor mass is much larger, especially for progenitor masses above ~ 5 M$_\odot$. The changes are due to differences in the WD cooling ages obtained with the different WD models. Both S00 and LPCODE models give WD ages consistent within the observational errors in $\log g$ and $T_{\rm eff}$, however the short lifetime of massive stars makes the determination of M_i very sensitive to small differences in $t_{\rm cool}$ for higher progenitor masses.

Figure 6 gives an overview of the relative contributions of observational and model (cooling tracks, including systematic effects due to variations of input physics and chemical stratification) uncertainties to the total error budget for the final WD masses and ages. We display also the relative contribution of cluster age (due to isochrones, cluster metallicity, reddening, distance) and WD age (due to cooling tracks) uncertainties to the total error budget for the progenitor masses and ages. These fractional contributions are expressed in terms of $(\sigma_i/\sigma_{\rm tot})^2$ for each WD, denoted by its number (as in Table 1), whilst vertical dashed lines separate the various clusters. The uncertainty of the WD mass appears to be completely dominated by the observational errors in $\log g$ and $T_{\rm eff}$, while in case of WD ages the systematic uncertainties of the cooling tracks dominate for some clusters (NGC3532 and NGC2099). For the progenitor ages and masses (lower panels of Fig. 6) cluster ages are the largest contributors to the total error, except mainly for NGC2099.

In closing this section, we comment on the possibility that systematic uncertainties (to be added to the quoted errors) may be present in the empirical determination of WDs $T_{\rm eff}$ and $\log g$ (see, e.g., Napiwotzki et al. 1999). We have not included this source of uncertainty in our global error assessment simply because it is not quantified in the literature. We have performed, however, a simple test to understand how such hypothetical uncertainties may influence the determinations of WD masses and cooling ages. We have considered that $T_{\rm eff}$ determinations have systematic uncertainties amounting up to ± 1000 K, that we represent by means of a uniform distribution. Analogously, in the case of $\log g$ we have assumed an additional systematic uncertainty of ± 0.15 dex. Note that these are probably very generous systematic errors, because we assume all WDs are similarly affected. Our

results show that uncertainties in $\log g$ have a more noticeable effect than those on T_{eff}. This is because WD masses are more robustly predicted by WD models than cooling ages, and consequently the error budget is dominated by observational uncertainties (as already shown in Fig. 6). For about 40% of our sample, uncertainties in WD masses are about a factor of 2 larger when systematic uncertainties as described above are included; these are the stars that show the smallest observational uncertainties in Table 1. For the rest of the stars in our sample, uncertainties are increased by not more than a factor of 1.5. Cooling ages, on the other hand, are much less affected by systematic uncertainties, because the total error budget here is heavily influenced by input physics and systematics in WD models. As a consequence, initial mass determinations are only very mildly affected. Indeed, the largest increase in positive uncertainties for M_i is only 50%, with only 4 objects having changes above 40%. There are 40 objects for which positive uncertainties increase by less than 25%. Negative uncertainties, which are always smaller, are less affected, and for 49 objects, increases are smaller than 25%. We thus conclude that adding systematic uncertainties to WD observational parameters would only have a very modest influence on the inferred IFMR. Based on these results and also considering that any attempt to quantify systematic uncertainties remains, at this point, arbitrary, we have chosen not to include these effects neither in our reference IFMR nor in the discussion of our results.

4.2. Comparison between predicted and derived IFMRs

Figure 3 compares the inferred IFMR with that predicted by the same BaSTI models (we chose to display the BaSTI results for [Fe/H]=0.06) used in the determination of t_{prog} and M_i. We display results obtained from progenitor models and isochrones with and without MS core overshooting.

Cluster ages determined from models without overshooting are smaller (see Table 3), hence t_{prog} is decreased, resulting in larger progenitor masses.

As a consequence, although the associated error bars are large, models without overshooting predict for some stars progenitors masses well above the maximum possible values allowed by theory. Examples are the WD in the Pleiades and two of the WDs in NGC2516 (see Table 6), for which the estimated progenitor masses are between ~ 12 and $\sim 16\,M_\odot$. Theoretical stellar evolution models predict an upper limit to the progenitors of carbon/oxygen white dwarfs in the range between ~ 6 and $\sim 8\,M_\odot$, the exact values depending on the chemical composition of the models and on the treatment of mixing in the cores; lower upper limits are obtained when core overshooting during the central H-burning phase is included. In several other cases in Table 6 even negative progenitor ages were obtained.

The relationship between M_i and the core mass at the onset of the thermal pulses (M_{c1TP}) is also displayed in Fig. 3. For models without core overshooting, the theoretical IFMR lies largely above the semi-empirical determination, especially for $M_i < 5\,M_\odot$, while the theoretical $M_i - M_{c1TP}$ relationship is in better agreement with the data. This would imply that the progenitor stars did not experience any thermal pulses at all.

On the other hand, for core overshooting models the theoretical IFMR follows much better the semi-empirical results, and no very high initial masses are typically derived in this case. The theoretical $M_i - M_{c1TP}$ relation constitutes a lower envelope to the data, consistent with general expectations about AGB evolution. This would lead us to conclude that core overshooting during the MS results in a better agreement with the derived IFMR, because of the internal consistency about the end-product of stars with inferred M_i.

Before moving forward in our comparison with theory, we wish to comment briefly on NGC2099, that represents an interesting case and a warning about the role played by the cluster [Fe/H] and E(B-V) estimates. As already mentioned, we have considered two possible values for its metallicity and reddening. Results for both choices are given in Table 6 and are also plotted in Fig. 7. It becomes apparent from the figure that data points fall systematically below even the theoretical $M_i - M_{c1TP}$ (models and IFMR with overshooting) relation for [Fe/H]= 0.09. The same result is obtained if models without core overshooting are used instead. This inconsistency is strongly alleviated if the alternative [Fe/H] and E(B-V) used by Kalirai et al. (2005, see Table 3) are adopted. While the aim of this paper is not to use the IFMR to improve cluster properties, this example demonstrates how informative it can be, when systematic effects are well controlled.

Focusing again on the core overshooting IFMR (Fig. 3, top panel) we can finally try to obtain some constraints on TP-AGB evolution by comparing the inferred IFMR with that resulting from sequences with different TP-AGB modelling. To do this, we first compare in Fig. 3 the $M_i - M_{c1TP}$ relations from BaSTI and LPCODE stellar models (thick dotted and thin dashed lines respectively). Both relations are very similar, regardless of differences in the treatment of convective and additional mixing episodes. We recall that in BaSTI instantaneous mixing in the overshooting region beyond the Schwarzschild boundary of the H-burning convective core is assumed, as well as semiconvective mixing during He-core burning, which is briefly described in Pietrinferni et al. (2004), where also the appropriate references are given. On the other hand, no extra mixing is taken into account at the bottom of convective envelopes. LPCODE models include diffusive mixing due to overshooting at all convective boundaries. We also point out that evolutionary timescales until the onset of the TPs are very similar in BaSTI models with overshooting and the LPCODE models. Since TP-AGB lifetimes are very short and their contribution to the the total progenitor

age can be neglected, we can safely use semi-empirical data obtained from BaSTI models for comparisons with the LPCODE theoretical IFMR.

Having assessed the similarity of the $M_{\rm i} - M_{\rm c1TP}$ relations, differences in the IFMRs predicted by BaSTI and LPCODE models can be traced to differences during the TP-AGB phase. While BaSTI models do not include extra mixing during the thermal pulses, LPCODE includes, as mentioned above, diffusive overshooting at all convective boundaries. The theoretical IFMRs are also shown in Fig. 3 with thick (BaSTI) and thin (LPCODE) solid lines and do indeed differ. This is unrelated to the choice of mass loss during the AGB phase, and it is mainly due to the presence of very strong third dredge-up episodes in LPCODE sequences, which inhibit the growth of the H-free core for models with $M_{\rm i} \gtrsim 3{\rm M}_\odot$. These strong third dredge-up episodes can be traced back mainly to the presence of overshooting at the base of the thermal pulse driven convective zone. This was demonstrated by Herwig (2000) and confirmed by us running test models where convective overshooting was included only at separately selected convective boundaries during the AGB evolution. Due to strong third dredge-up events, the final mass of LPCODE sequences with $M_{\rm i} \gtrsim 3M_\odot$ is very similar to $M_{\rm c1TP}$, the core mass at the first thermal pulse (Fig. 3, top panel). On the other hand in BaSTI sequences the final mass is mainly set by the length of the TP-AGB phase and, thus, by the adopted mass loss rate. The apparent failure of the theoretical LPCODE IFMR to match the final masses in the range $2.75M_\odot \lesssim M_{\rm i} \lesssim 3.5M_\odot$ is an indication that such strong dredge-up episodes do not take place in real stars, and therefore the adopted exponentially decaying overshooting at the base of the thermal pulse driven convective zone in the LPCODE models is too strong. This allows us to conclude that the overshooting parameter f (see Herwig et al. 1997, for a definition of f) must be significantly smaller than $f = 0.016$ employed at the convective core of upper MS stars. This is in line with recent hydrodynamical simulations of AGB thermal pulses which point to a value of $f \lesssim 0.01$ at the bottom of the pulse driven convective zone (Herwig et al. 2007). On the other hand, given the large error bars of the data points, the existence of strong third dredge-up episodes for stars with $M_{\rm i} \gtrsim 5M_\odot$ cannot be excluded by the same arguments. The IFMR may therefore teach us that overshooting varies a lot between different convective layers and may also depend on stellar mass.

5. Summary and conclusions

Since its earliest determination, the semi-empirical IFMR has indicated a monotonic rise of the final WD mass with the initial mass of the progenitor. It is also strong evidence that single stars of intermediate mass do not develop degenerate cores close to the

Chandrasekhar limit, most likely due to the effect of strong mass loss on the AGB. These qualitative results have remained unchanged in spite of the significant improvement both in the amount and accuracy of observational data and in the theoretical models. Nevertheless there are still many open questions, such as a dependence on metallicity, the slope of the IFMR at the upper (initial) mass end, changes in slope, and spread around a mean relation. To answer these questions, not only increasingly accurate observations are needed, but also the systematic uncertainties coming from the theoretical input – which is necessary to establish the semi-empirical IFMR – have to be controlled. These are related to evolutionary tracks and isochrones that determine the total age of the observed WDs and cooling tracks used for deriving the WD age. Our paper was intended to investigate the influence of such systematic uncertainties and to derive robust features of the IFMR. We also investigated what uncertainties in the theory of stellar evolution would lead to inconsistent results, and therefore could be restricted or excluded.

From the available WD data we selected a total of 52 objects in 10 open clusters, plus Sirius B. There are, in fact, even more objects available, but we disregarded those for which our cluster distance determination (Sect. 2) would not be possible because of the lack of calibrating field stars at that metallicity (NGC6791 at [Fe/H] = 0.45). We also did not take into account the objects from Catalán et al. (2008b), because of the more indirect way to obtain the age of the mostly unevolved binary companion. Inclusion of such objects would weaken our aim of highest possible self-consistency.

For the determination of mass and cooling age of the WDs we used different sets of cooling track, from Salaris et al. (2000) and the LPCODE (Althaus et al. 2003) to evaluate the influence of different codes, input physics and chemical stratification (Sect. 3.1). We estimated the error ranges quite conservatively and to evaluate the global error budget we used Monte Carlo simulations (Sect. 3.3), for which we assumed either a normal or uniform distribution of the different error sources. We included the effect of observational errors, too.

Results concerning cooling ages and final masses are quite robust: the accuracy of the WD masses depend completely on the observational uncertainties, while their ages is influenced in most cases (in terms of number of clusters) by the uncertainties of the cooling tracks, mostly systematic differences between different sets of cooling tracks and changes in the neutrino emission rates.

This result implies that any spread in M_f, as seen in Fig. 2, which is outside the error bar is real, in the sense that M_f does vary at the same (within the errors in M_i) initial mass. Whether this spread is consistent with theoretical expectations, related to a steep increase of M_f with M_i in that mass range, or whether it is due to star-to-star variations in the total mass lost, cannot be decided yet, as the error bars in M_i are too large even in the case of

the Praesepe WDs, which we discussed in detail in Sect. 2.4.

Figure 5 demonstrates that uncertainties due to different WD codes with similar, but not identical physics and model details are essentially irrelevant for the estimate of M_f. However, differences in the cooling ages have a significant influence on M_i, since they affect directly progenitor lifetimes, and the more massive progenitors evolve on very short timescales. Therefore the two different sets of cooling tracks lead to quite different values for M_i, particularly for initial masses above 5 $M_\odot$. In this regime, M_i differences are between $\sim$ 0.5 and 2.0 $M_\odot$.

The determination of M_i is more complex, as it involves several steps. The age determination of the cluster or binary system requires metallicity, reddening and distance. We have used literature values for the former two, and our own homogenous determination for the latter. Uncertainties from both steps have been taken into account. Using appropriate isochrones the age is then obtained, which, together with the WD cooling age, results in the pre-WD lifetime. As this is, to an accuracy of 1% or slightly more, identical to the lifetime from the MS to the end of the central He-burning phase, all uncertainties concerning the AGB evolution are irrelevant. We employed different sets of stellar models (Pietrinferni et al. 2004; Girardi et al. 2000), which differ slightly in the detailed treatment of the input physics (but both include core overshooting during the MS) as well as additional models from the former source (BaSTI), which do not consider convective overshooting. The first effect – different tracks – has a very minor effect on M_i, as we showed in Fig. 4. Note that this includes both the cluster age determination and the relation between progenitor age and mass. The neglect of overshooting, however, leads to internal inconsistencies in the semi-empirical IFMR: at the high end, initial masses are predicted, for which the models themselves predict that no electron degenerate CO-WD would result from the evolution. By discriminating between the different error sources (but omitting the overshooting effect), Fig. 6 demonstrates that the cluster age uncertainties (due to uncertainties in the cluster [Fe/H] and reddening estimates) dominate the error on M_i, although the above-mentioned WD age can be significant for the more massive progenitors, too.

The case of NGC2099 illustrates the importance of accurate metallicities and reddenings: Figure 7 shows how drastically the semi-empirical IFMR changes, two different estimates of [Fe/H] and $E(B-V)$ are assumed. If one accepts this uncertainty as being real, NGC2099 cannot be used at all to learn about the IFMR.

After we had determined the full extent of the uncertainty associated to our semi-empirical IFMR, we compared it with the predictions from the theoretical calculations, both from BaSTI and LPCODE. Both differ in their treatment of convective overshooting during the AGB phase. One should recall that the BaSTI models treat that phase with

synthetic models, while LPCODE follows the evolution in full detail. Figure 3 shows them in comparison with the semi-empirical IFMR and the relation between M_i and the mass of the CO-core at the first thermal pulse, M_{c1TP}. As long as stars do not avoid the AGB phase, $M_f \geq M_{c1TP}$ should be fulfilled. Therefore, this relation is a strong lower limit to the semi-empirical IFMR. The agreement between the $M_i - M_{c1TP}$ relations from both codes is excellent; there are no significant systematic uncertainties in its prediction. This again emphasizes the need for convective overshooting during the MS phase: without it a significantly larger numbers of objects falls below this limiting line.

On the other hand, the theoretical IFMR from the LPCODE tracks is not consistent with the data: In these models overshooting during the AGB, mainly from the lower boundary of the pulse-driven convective zone, limits the growth of the CO-core such that the final core size is almost identical to that at the first pulse. However, most objects have final masses clearly above this line, such that we concluded that the extent of overshooting during the AGB phase must be significantly smaller than on the MS. This is in agreement with hydrodynamical simulations.

The theoretical IFMRs displayed in Figure 3, and in particular those resulting from the BaSTI models display the largest gradient in the same mass range where a significant spread in M_f is observed. We demonstrated that indeed that spread could arise solely from this local steep gradient, such that no other explanation would be needed. If it is not, one would have to invoke a spread in the total mass lost in a given, small mass range. This is not exceptional, as the morphology of horizontal branches in Galactic globular cluster shows, but the reasons for such a star-to-star variation are unclear. In other mass ranges the total error budget is too large to discuss the reality and reason for apparent spreads in M_f.

Figure 2 presents our reference semi-empirical IFMR, obtained using BaSTI isochrones and tracks with overshooting and S00 cooling models. The error bars include all errors we have investigated. Compared to Ferrario et al. (2005) our error bars are necessarily larger (we consider more sources of error), but on average only by less than a factor of two, and mostly for M_i. We also present a simple linear fit through all the data as well as a piecewise fit, which reflects the properties of the theoretical IFMR based on the BaSTI models.

In summary, our most important results are

1. None of the WDs employed in current IFMR determinations is close to the Chandrasekhar mass, not even the progeny of the more massive intermediate mass stars;

2. stellar models without convective overshooting during core hydrogen burning lead to internal inconsistencies in the semi-empirical IFMR;

3. overshooting from convective boundaries during the AGB phase must be significantly reduced (compared to the case of convective cores along the MS) to reproduce the observed M_f values;

4. the uncertainty in M_f is dominated by observational errors;

5. the uncertainty in M_i has several reasons: both cluster parameters and isochrone details influence the cluster age and thus the progenitor mass; the uncertainty on the WD cooling age can sometimes also be the dominant factor;

6. the observed dispersion in M_f at approximately constant M_i (3.0–3.5 $M_\odot$), in particular for the Praesepe objects, appears to be real. It may follow from the steep increase of M_f with M_i predicted by theoretical IFMRs in that M_i range, rather than being caused by a spread in mass loss among cluster AGB stars;

7. from the general agreement between the theoretical IFMRs and the semiempirical data, we find no evidence that the mass loss prescriptions used in the stellar evolution calculations grossly disagree with the total mass actually lost by low- and intermediate-mass stars;

8. the case of NGC2099 illustrates the necessity for accurate cluster parameters; reliable composition data and reddening are required;

9. as long as up-to-date input physics is used for the stellar models, systematic uncertainties do not change the overall appearance of the semi-empirical IFMR as determined recently by several groups.

An extension of this analysis to a larger range of [Fe/H] is needed, to investigate a possible metallicity dependence of the IFMR, given the small [Fe/H] range spanned by the systems analyzed in this study (see Table 3). In addition to the relevant observational data, this requires also a careful study of how to extend to a wider [Fe/H] range the empirical MS fitting technique adopted here to determine cluster distances, if we wish to maintain the same degree of homogeneity in the derivation of the cluster ages. An extension to lower metallicities seems to be preferable, as both calibrating objects and suitable clusters should exist, contrary to the case of an extension to higher, that is super-solar clusters.

As most of the clusters used for deriving the IFMR have nearly solar metallicities, the question arises, what the true solar chemical composition is? Asplund et al. (2005) have presented new determinations of the solar heavy element abundance, drastically lower than the standard composition assumed here and in the stellar evolution tracks employed. Both BaSTI and LPCODE progenitor models consider a standard solar mixture with $Z/X \sim 0.0245$,

whereas Asplund et al. (2005) redetermination gives $Z/X \sim 0.0165$. Assuming that the differential abundance analyses for our open cluster sample provides the true abundances relative to the sun, also the clusters should be less metal-rich than thought. It would be interesting to see how this will affect the semi-empirical IFMR and its agreement with theoretical predictions. An extension of this investigation by using in the computation of progenitor models the new solar abundances is currently under way.

REFERENCES

Althaus, L. G., Serenelli, A. M., Córsico, A. H., & Montgomery, M. H. 2003, A&A, 404, 593

Asplund, M., Grevesse, N., & Sauval, A. J. 2005, in Astronomical Society of the Pacific Conference Series, Vol. 336, Cosmic Abundances as Records of Stellar Evolution and Nucleosynthesis, ed. T. G. Barnes, III & F. N. Bash, 25–+

Barstow, M. A., Bond, H. E., Holberg, J. B., Burleigh, M. R., Hubeny, I., & Koester, D. 2005, MNRAS, 362, 1134

Bischoff-Kim, A., Montgomery, M. H., & Winget, D. E. 2008, ApJ, 675, 1512

Bragaglia, A., Carretta, E., Gratton, R. G., Tosi, M., Bonanno, G., Bruno, P., Calì, A., Claudi, R., Cosentino, R., Desidera, S., Farisato, G., Rebeschini, M., & Scuderi, S. 2001, AJ, 121, 327

Cassisi, S., Potekhin, A. Y., Pietrinferni, A., Catelan, M., & Salaris, M. 2007, ApJ, 661, 1094

Castanheira, B. G. & Kepler, S. O. 2008, MNRAS, 385, 430

Catalán, S., Isern, J., García-Berro, E., & Ribas, I. 2008a, MNRAS, 387, 1693

Catalán, S., Isern, J., García-Berro, E., Ribas, I., Allende Prieto, C., & Bonanos, A. Z. 2008b, A&A, 477, 213

Chen, L., Hou, J. L., & Wang, J. J. 2003, AJ, 125, 1397

Claver, C. F., Liebert, J., Bergeron, P., & Koester, D. 2001, ApJ, 563, 987

Deliyannis, C. P., Jacobson, H., Cummings, J., Steinhauer, A., & Sarajedini, A. 2002, in Bulletin of the American Astronomical Society, Vol. 34, Bulletin of the American Astronomical Society, 1308–+

Dobbie, P. D., Napiwotzki, R., Burleigh, M. R., Barstow, M. A., Boyce, D. D., Casewell, S. L., Jameson, R. F., Hubeny, I., & Fontaine, G. 2006a, MNRAS, 369, 383

Dobbie, P. D., Napiwotzki, R., Lodieu, N., Burleigh, M. R., Barstow, M. A., & Jameson, R. F. 2006b, MNRAS, 373, L45

Dobbie, P. D., Pinfield, D. J., Napiwotzki, R., Hambly, N. C., Burleigh, M. R., Barstow, M. A., Jameson, R. F., & Hubeny, I. 2004, MNRAS, 355, L39

Dominguez, I., Straniero, O., Tornambe, A., & Isern, J. 1996, ApJ, 472, 783

Fernandez, J. A. & Salgado, C. W. 1980, A&AS, 39, 11

Ferrario, L., Wickramasinghe, D., Liebert, J., & Williams, K. A. 2005, MNRAS, 361, 1131

Fontaine, G., Brassard, P., & Bergeron, P. 2001, PASP, 113, 409

Gim, M., Vandenberg, D. A., Stetson, P. B., Hesser, J. E., & Zurek, D. R. 1998, PASP, 110, 1318

Girardi, L., Bertelli, G., Bressan, A., Chiosi, C., Groenewegen, M. A. T., Marigo, P., Salasnich, B., & Weiss, A. 2002, A&A, 391, 195

Girardi, L., Bressan, A., Bertelli, G., & Chiosi, C. 2000, A&AS, 141, 371

Gratton, R. 2000, in Astronomical Society of the Pacific Conference Series, Vol. 198, Stellar Clusters and Associations: Convection, Rotation, and Dynamos, ed. R. Pallavicini, G. Micela, & S. Sciortino, 225–+

Gratton, R., Bragaglia, A., Carretta, E., & Tosi, M. 2006, ApJ, 642, 462

Grevesse, N. & Noels, A. 1993, in Origin and Evolution of the Elements, ed. S. Kubono & T. Kajino, 14–+

Haft, M., Raffelt, G., & Weiss, A. 1994, ApJ, 425, 222

Herwig, F. 2000, A&A, 360, 952

Herwig, F., Bloecker, T., Schoenberner, D., & El Eid, M. 1997, A&A, 324, L81

Herwig, F., Freytag, B., Fuchs, T., Hansen, J. P., Hueckstaedt, R. M., Porter, D. H., Timmes, F. X., & Woodward, P. R. 2007, in Astronomical Society of the Pacific Conference Series, Vol. 378, Why Galaxies Care About AGB Stars: Their Importance as Actors and Probes, ed. F. Kerschbaum, C. Charbonnel, & R. F. Wing, 43–+

Iben, Jr., I. & Renzini, A. 1983, ARA&A, 21, 271

Isern, J., García-Berro, E., Torres, S., & Catalán, S. 2008, ApJ, 682, L109

Itoh, N., Hayashi, H., & Kohyama, Y. 1993, ApJ, 418, 405

Itoh, N., Hayashi, H., Nishikawa, A., & Kohyama, Y. 1996, ApJS, 102, 411

Johnson, H. L. 1952, ApJ, 116, 640

Johnson, H. L. & Knuckles, C. F. 1955, ApJ, 122, 209

Johnson, H. L. & Mitchell, R. I. 1958, ApJ, 128, 31

Jones, B. F. & Prosser, C. F. 1996, AJ, 111, 1193

Kalirai, J. S., Hansen, B. M. S., Kelson, D. D., Reitzel, D. B., Rich, R. M., & Richer, H. B. 2008, ApJ, 676, 594

Kalirai, J. S., Richer, H. B., Fahlman, G. G., Cuillandre, J.-C., Ventura, P., D'Antona, F., Bertin, E., Marconi, G., & Durrell, P. R. 2001a, AJ, 122, 266

Kalirai, J. S., Richer, H. B., Reitzel, D., Hansen, B. M. S., Rich, R. M., Fahlman, G. G., Gibson, B. K., & von Hippel, T. 2005, ApJ, 618, L123

Kalirai, J. S., Ventura, P., Richer, H. B., Fahlman, G. G., Durrell, P. R., D'Antona, F., & Marconi, G. 2001b, AJ, 122, 3239

Koester, D. & Reimers, D. 1993, A&A, 275, 479

—. 1996, A&A, 313, 810

Koester, D. & Weidemann, V. 1980, A&A, 81, 145

Liebert, J., Young, P. A., Arnett, D., Holberg, J. B., & Williams, K. A. 2005, ApJ, 630, L69

Loktin, A. V., Gerasimenko, T. P., & Malishev, L. K. 2001, Astron. Astrophys. Trans., 20, 607

Marigo, P. & Girardi, L. 2007, A&A, 469, 239

Meynet, G., Mermilliod, J.-C., & Maeder, A. 1993, A&AS, 98, 477

Mochejska, B. J. & Kaluzny, J. 1999, Acta Astronomica, 49, 351

Morel, P. 1997, A&AS, 124, 597

Napiwotzki, R., Green, P. J., & Saffer, R. A. 1999, ApJ, 517, 399

Nilakshi & Sagar, R. 2002, A&A, 381, 65

Percival, S. M. & Salaris, M. 2003, MNRAS, 343, 539

Percival, S. M., Salaris, M., & Groenewegen, M. A. T. 2005, A&A, 429, 887

Percival, S. M., Salaris, M., & Kilkenny, D. 2003, A&A, 400, 541

Perryman, M. A. C., Brown, A. G. A., Lebreton, Y., Gomez, A., Turon, C., de Strobel, G. C., Mermilliod, J. C., Robichon, N., Kovalevsky, J., & Crifo, F. 1998, A&A, 331, 81

Pietrinferni, A., Cassisi, S., Salaris, M., & Castelli, F. 2004, ApJ, 612, 168

Prada Moroni, P. G. & Straniero, O. 2007, A&A, 466, 1043

Press, W. H., Teukolsky, S. A., Vetterling, W. T., & Flannery, B. P. 1992, Numerical recipes in FORTRAN. The art of scientific computing (Cambridge: University Press, —c1992, 2nd ed.)

Provencal, J. L., Shipman, H. L., Hog, E., & Thejll, P. 1998, ApJ, 494, 759

Raffelt, G. G. 1996, Stars as laboratories for fundamental physics: the astrophysics of neutrinos, axions, and other weakly interacting particles (Chicago, University of Chicago Press)

Reid, I. N. 1996, AJ, 111, 2000

Rubin, K. H. R., Williams, K. A., Bolte, M., & Koester, D. 2008, AJ, 135, 2163

Salaris, M., Cassisi, S., García-Berro, E., Isern, J., & Torres, S. 2001, A&A, 371, 921

Salaris, M., Dominguez, I., Garcia-Berro, E., Hernanz, M., Isern, J., & Mochkovitch, R. 1997, ApJ, 486, 413

Salaris, M., García-Berro, E., Hernanz, M., Isern, J., & Saumon, D. 2000, ApJ, 544, 1036

Schaller, G., Schaerer, D., Meynet, G., & Maeder, A. 1992, A&AS, 96, 269

Schuler, S. C., King, J. R., Fischer, D. A., Soderblom, D. R., & Jones, B. F. 2003, AJ, 125, 2085

Serenelli, A. M. & Fukugita, M. 2007, ApJS, 172, 649

Straniero, O., Domínguez, I., Imbriani, G., & Piersanti, L. 2003, ApJ, 583, 878

Sung, H. & Bessell, M. S. 1999, MNRAS, 306, 361

Sung, H., Bessell, M. S., Lee, B.-W., & Lee, S.-G. 2002, AJ, 123, 290

von Hippel, T. 2005, ApJ, 622, 565

Wagenhuber, J. & Groenewegen, M. A. T. 1998, A&A, 340, 183

Weidemann, V. 1977, A&A, 59, 411

—. 1987, A&A, 188, 74

—. 2000, A&A, 363, 647

Weidemann, V. & Koester, D. 1983, A&A, 121, 77

Williams, K. A., Bolte, M., & Koester, D. 2004, ApJ, 615, L49

Table 1.   Adopted data for our WD sample, taken from the literature (see Sect. 2.1).

System	WD name	$T_{\rm eff}$ [K]	$\sigma(T_{\rm eff})$	$\log(g)$ [cm s^{-2}]	$\sigma(\log(g))$	ID
Pleiades	LB1497	32841	170	8.630	0.040	1
Hyades	0352+098	16630	350	8.160	0.050	2
	0406+169	15180	350	8.300	0.050	3
	0421+162	19570	350	8.090	0.050	4
	0425+168	24420	350	8.110	0.050	5
	0431+125	21340	350	8.040	0.050	6
	0438+108	27390	350	8.070	0.050	7
	0437+138	15340	350	8.260	0.050	8
Praesepe	0836+197	21950	350	8.450	0.050	9
	0836+201	16630	350	8.010	0.050	10
	0836+199	14060	630	8.340	0.060	11
	0837+199	17100	350	8.320	0.050	12
	0837+218	16833	250	8.390	0.030	13
	0837+185	14748	400	8.240	0.050	14
	0840+200	14180	350	8.230	0.050	15
	0833+194	14999	250	8.180	0.040	16
	0840+190	14765	270	8.210	0.030	17
	0840+205	14527	390	8.240	0.040	18
	0843+184	14498	200	8.220	0.040	19
NGC2516	2516-1	28170	310	8.480	0.170	20
	2516-2	34200	610	8.600	0.110	21
	2516-3	26870	330	8.550	0.070	22
	2516-5	30760	420	8.700	0.120	23
NGC3532	3532-8	23370	1065	7.713	0.148	24
	3532-9	29800	616	7.827	0.229	25
	3532-10	19270	974	8.143	0.266	26
NGC2099 (M37)	2099-WD2	19900	900	8.110	0.160	27
	2099-WD3	18300	900	8.230	0.210	28
	2099-WD4	16900	1100	8.400	0.260	29
	2099-WD5	18300	1000	8.330	0.220	30
	2099-WD7	17800	1400	8.420	0.320	31

Table 1—Continued

System	WD name	T_{eff} [K]	$\sigma(T_{\text{eff}})$	$\log(g)$ [cm s^{-2}]	$\sigma(\log(g))$	ID
	2099-WD9	15300	400	8.000	0.080	32
	2099-WD10	19300	400	8.200	0.070	33
	2099-WD11	23000	600	8.540	0.100	34
	2099-WD12	13300	1000	7.910	0.120	35
	2099-WD13	18200	400	8.270	0.080	36
	2099-WD14	11400	200	7.730	0.160	37
	2099-WD16	13100	500	8.340	0.100	38
NGC2168 (M35)	NGC2168 LAWDS1	32400	512	8.400	0.125	39
	NGC2168 LAWDS 2	32700	603	8.340	0.080	40
	NGC2168 LAWDS 5	52600	1160	8.240	0.095	41
	NGC2168 LAWDS 6	55200	897	8.280	0.065	42
	NGC2168 LAWDS 15	29900	318	8.480	0.060	43
	NGC2168 LAWDS 27	30500	397	8.520	0.061	44
Sirius	Sirius B	25193	37	8.566	0.010	45
NGC7789	NGC 7789-5	31213	238	7.904	0.054	46
	NGC 7789-8	24319	447	8.004	0.066	47
	NGC 7789-9	20939	727	7.838	0.115	48
NGC6819	NGC 6819-6	21094	252	7.832	0.036	49
	NGC 6819-7	15971	197	7.908	0.038	50
NGC 1039	NGC1039 LAWDS 15	25900	1100	8.380	0.120	51
	NGC1039 LAWDS 17	24700	1100	8.440	0.120	52
	NGC1039 LAWDS S2	31200	1100	8.320	0.120	53

Table 2.   Sources of the data used for determining the cluster ages.

Name	[Fe/H]	E(B-V)	CMD
Pleiades	Gratton (2000)	Percival et al. (2003)	Johnson & Mitchell (1958)
Hyades	Gratton (2000)		Johnson & Knuckles (1955)
Praesepe	Gratton (2000)		Johnson (1952)
NGC2516	Gratton (2000)	Loktin et al. (2001)	Sung et al. (2002)
NGC3532	Gratton (2000)	Loktin et al. (2001)	Fernandez & Salgado (1980)
NGC2099 (M37)	Chen et al. (2003)	Loktin et al. (2001)	Nilakshi & Sagar (2002)
NGC2168 (M35)	Gratton (2000)	Loktin et al. (2001)	Sung & Bessell (1999)
NGC7789	Gratton (2000)	Percival & Salaris (2003)	Mochejska & Kaluzny (1999)
NGC6819	Bragaglia et al. (2001)	Bragaglia et al. (2001)	Kalirai et al. (2001a)
NGC1039	Schuler et al. (2003)	Loktin et al. (2001)	Jones & Prosser (1996)

Table 3.   Cluster ages determined from the adopted metallicities, reddening values and
derived distance moduli, using three different sets of isochrones.

Name	[Fe/H]	E(B − V)	$(m − M)_V$	Age[Myr][a]	Age[Myr][b]	Age[Myr][c]
Pleiades	-0.03 ± 0.06	0.04	5.74±0.05	50±10	85±10	95±10
Hyades	0.13 ± 0.06	0.0	3.33±0.01	440±40	640±40	630±40
Praesepe	0.04 ± 0.06	0.0	6.24±0.04	450±40	650±50	640±40
NGC2516	-0.16 ± 0.11	0.10	8.27±0.07	85±45	130±50	140±50
NGC3532	0.02 ± 0.06	0.04	8.40±0.25	300±100	400±100	400±100
NGC2099 (M37) [d]	0.09 ± 0.15	0.30	12.00±0.12	220±30	320±30	320±30
	-0.20	0.23	11.40±0.12	350±40	550±50	540±50
NGC2168 (M35)	-0.19 ± 0.15	0.26	10.50±0.12	85±25	120±30	130±30
NGC7789	-0.13 ± 0.08	0.29	12.12±0.12	1100±100	1500±100	1600±100
NGC6819	0.09 ± 0.03	0.14 ± 0.04	12.60±0.20	1500±200	2000±200	2000±200
NGC1039	0.07 ± 0.04	0.07	8.80±0.15	150±30	250±25	250±25
Sirius A		0.0	——	181±30	170±50	170±25

[a]Ages from BaSTI isochrones without overshooting

[b]Ages from BaSTI isochrones with overshooting

[c]Ages from Padua isochrones with overshooting

[d]For NGC2099 a second alternative [Fe/H] value was tested (see text for details)

Table 4.   Fractional $1 - \sigma$ uncertainties in WD mass and cooling age for relevant WD input physics, as functions of effective temperature and surface gravity.

log(g) [cm s^{-2}] = log($T_{\rm eff}$) [K]	Fract. uncert. for WD mass					Fract. uncert. for WD cooling age				
	8.6	8.4	8.2	8.0	7.8	8.6	8.4	8.2	8.0	7.8
Cooling tracks										
4.60	0.017	0.015	0.016	0.016	0.003	0.826	0.564	0.287	0.335	0.377
4.45	0.016	0.015	0.014	0.010	0.011	0.036	0.262	0.291	0.174	0.006
4.30	0.015	0.014	0.013	0.007	0.017	0.072	0.064	0.012	0.057	0.159
4.15	0.012	0.012	0.011	0.003	0.037	0.035	0.114	0.080	0.029	0.100
4.00	0.009	0.006	0.010	0.000	0.061	0.368	0.020	0.073	0.064	0.122
Neutrino cooling										
4.60	0.000	0.001	0.001	0.002	0.003	0.700	0.396	0.320	0.269	0.217
4.45	0.000	0.000	0.000	0.001	0.001	0.147	0.349	0.474	0.374	0.305
4.30	0.000	0.000	0.000	0.000	0.000	0.042	0.075	0.137	0.250	0.326
4.15	0.000	0.000	0.000	0.000	0.000	0.017	0.027	0.044	0.072	0.098
4.00	0.000	0.000	0.000	0.000	0.000	0.007	0.011	0.018	0.027	0.037
Conductive opacity										
4.60	0.000	0.000	0.000	0.001	0.001	0.391	0.095	0.040	0.022	0.020
4.45	0.000	0.000	0.001	0.001	0.002	0.056	0.197	0.200	0.089	0.046
4.30	0.000	0.000	0.000	0.001	0.002	0.033	0.009	0.028	0.083	0.090
4.15	0.000	0.000	0.000	0.000	0.001	0.056	0.049	0.040	0.024	0.035
4.00	0.000	0.000	0.000	0.000	0.000	0.067	0.058	0.054	0.053	0.083
Core composition										
4.60	0.002	0.002	0.002	0.002	0.002	0.058	0.046	0.043	0.046	0.066
4.45	0.002	0.002	0.002	0.002	0.002	0.013	0.042	0.040	0.043	0.047
4.30	0.002	0.001	0.001	0.002	0.002	0.003	0.028	0.036	0.040	0.043
4.15	0.002	0.001	0.001	0.001	0.002	0.005	0.013	0.033	0.037	0.039
4.00	0.002	0.001	0.001	0.001	0.002	0.001	0.007	0.029	0.037	0.039
H-envelope thickness										
4.60	0.006	0.008	0.012	0.014	0.020	0.035	0.003	0.011	0.001	0.024
4.45	0.005	0.007	0.010	0.013	0.021	0.029	0.015	0.007	0.004	0.014
4.30	0.005	0.006	0.009	0.012	0.024	0.033	0.011	0.005	0.013	0.006
4.15	0.004	0.006	0.008	0.011	0.027	0.028	0.027	0.007	0.008	0.015

Table 4—Continued

log(g) [cm s^{-2}] =	Fract. uncert. for WD mass					Fract. uncert. for WD cooling age				
log($T_{\rm eff}$) [K]	8.6	8.4	8.2	8.0	7.8	8.6	8.4	8.2	8.0	7.8
4.00	0.003	0.005	0.007	0.010	0.028	0.070	0.057	0.044	0.025	0.016

[a]Columns and rows are labeled according to $\log{(g)}$ and $\log{(T_{\rm eff})}$ respectively. Definitions of how the uncertainties were computed are given in Eqs. 3-7. Note, however, that for the sake of readability, uncertainties given here are linear (not logarithmic) in mass and cooling age and have been assumed symmetric. Fractional uncertainties smaller than 0.001 are shown as null values.

Table 5. White dwarf cooling ages and associated mass (in solar mass units) determined with the S00 cooling tracks. The bolometric luminosity is obtained using the derived cluster distances.

ID	$\log t_{\rm cool}$ [yr]	$\sigma_-(\log t_{\rm cool})$	$\sigma_+(\log t_{\rm cool})$	$M_{\rm f}[M_\odot]$	$\sigma_-(M_{\rm f})$	$\sigma_+(M_{\rm f})$	$\log(L/L_\odot)$
Pleiades							
1	7.667	-0.185	0.162	1.028	-0.031	0.031	-1.162
Hyades							
2	8.262	-0.063	0.056	0.713	-0.031	0.031	-2.032
3	8.466	-0.066	0.064	0.798	-0.032	0.033	-2.282
4	7.981	-0.105	0.086	0.679	-0.031	0.031	-1.701
5	7.585	-0.185	0.174	0.699	-0.031	0.031	-1.324
6	7.783	-0.146	0.130	0.652	-0.032	0.032	-1.518
7	7.274	-0.186	0.184	0.684	-0.032	0.031	-1.094
8	8.425	-0.063	0.061	0.773	-0.032	0.033	-2.237
Praesepe							
9	8.113	-0.072	0.065	0.901	-0.034	0.034	-1.739
10	8.159	-0.076	0.066	0.622	-0.028	0.032	-1.942
11	8.584	-0.086	0.085	0.820	-0.040	0.039	-2.443
12	8.338	-0.064	0.062	0.812	-0.034	0.034	-2.087
13	8.408	-0.058	0.057	0.857	-0.023	0.022	-2.161
14	8.459	-0.064	0.063	0.759	-0.032	0.033	-2.294
15	8.498	-0.062	0.062	0.751	-0.033	0.033	-2.357
16	8.402	-0.053	0.051	0.722	-0.026	0.027	-2.226
17	8.439	-0.052	0.051	0.740	-0.021	0.021	-2.273
18	8.476	-0.061	0.061	0.759	-0.027	0.027	-2.320
19	8.467	-0.054	0.053	0.746	-0.027	0.027	-2.311
NGC2516							
20	7.746	-0.298	0.192	0.926	-0.106	0.105	-1.323
21	7.543	-0.364	0.297	1.008	-0.071	0.070	-1.069
22	7.888	-0.116	0.087	0.970	-0.045	0.045	-1.455
23	7.858	-0.202	0.154	1.075	-0.078	0.078	-1.326
NGC3532							
24	7.373	-0.216	0.219	0.482	-0.085	0.076	-1.164
25	7.064	-0.303	0.161	0.563	-0.169	0.145	-0.789
26	8.047	-0.284	0.213	0.708	-0.150	0.164	-1.762

Table 5—Continued

ID	$\log t_{\rm cool}$ [yr]	$\sigma_-(\log t_{\rm cool})$	$\sigma_+(\log t_{\rm cool})$	$M_{\rm f}[M_\odot]$	$\sigma_-(M_{\rm f})$	$\sigma_+(M_{\rm f})$	$\log(L/L_\odot)$
NGC2099 (M37)							
27	7.971	−0.215	0.150	0.690	−0.093	0.096	−1.685
28	8.185	−0.193	0.167	0.759	−0.128	0.133	−1.909
29	8.411	−0.214	0.245	0.864	−0.163	0.164	−2.161
30	8.260	−0.190	0.194	0.821	−0.135	0.139	−1.975
31	8.366	−0.268	0.305	0.877	−0.198	0.203	−2.085
32	8.264	−0.083	0.072	0.614	−0.044	0.051	−2.082
33	8.090	−0.094	0.074	0.742	−0.044	0.044	−1.796
34	8.111	−0.108	0.097	0.959	−0.065	0.064	−1.720
35	8.380	−0.133	0.120	0.561	−0.080	0.067	−2.275
36	8.222	−0.082	0.075	0.783	−0.050	0.052	−1.945
37	8.455	−0.125	0.121	0.448	−0.129	0.123	−2.461
38	8.667	−0.097	0.103	0.818	−0.064	0.066	−2.567
NGC2168 (M35)							
39	7.343	−0.339	0.355	0.884	−0.078	0.079	−1.021
40	7.223	−0.310	0.327	0.849	−0.051	0.050	−0.962
41	6.351	−0.213	0.208	0.820	−0.055	0.056	−0.052
42	6.292	−0.218	0.217	0.845	−0.041	0.040	+0.006
43	7.634	−0.219	0.200	0.928	−0.040	0.040	−1.219
44	7.644	−0.215	0.186	0.955	−0.041	0.041	−1.212
Sirius B							
45	7.996	−0.063	0.062	0.978	−0.016	0.016	−1.580
NGC7789							
46	6.998	−0.137	0.135	0.601	−0.028	0.029	−0.757
47	7.480	−0.181	0.179	0.637	−0.037	0.039	−1.265
48	7.627	−0.205	0.192	0.543	−0.059	0.058	−1.428
NGC6819							
49	7.609	−0.153	0.150	0.540	−0.021	0.019	−1.412
50	8.141	−0.071	0.063	0.566	−0.023	0.021	−1.951
NGC1039							
51	7.801	−0.239	0.161	0.863	−0.075	0.075	−1.443

Table 5—Continued

ID	$\log t_{\rm cool}$ [yr]	$\sigma_-(\log t_{\rm cool})$	$\sigma_+(\log t_{\rm cool})$	$M_{\rm f}[M_\odot]$	$\sigma_-(M_{\rm f})$	$\sigma_+(M_{\rm f})$	$\log(L/L_\odot)$
52	7.934	-0.179	0.126	0.899	-0.076	0.076	-1.533
53	7.308	-0.312	0.339	0.834	-0.072	0.076	-1.144

Table 6.   Initial–final–mass-relation obtained by combining BaSTI progenitor models with and without overshooting (indicated by OV resp. non-OV) with S00 WD tracks [a] .

ID	$M_{\rm f}[M_\odot]$	$\sigma(M_{\rm f})$	OV models			non-OV models		
			$M_{\rm i}[M_\odot]$	$\sigma_-(M_{\rm i})$	$\sigma_+(M_{\rm i})$	$M_{\rm i}[M_\odot]$	$\sigma_-(M_{\rm i})$	$\sigma_+(M_{\rm i})$
Pleiades								
1	1.028	0.031	7.847	−1.257	3.069	15.52	−3.986	99.90
Hyades								
2	0.713	0.031	3.067	−0.100	0.107	3.690	−0.192	0.224
3	0.798	0.032	3.383	−0.174	0.208	4.438	−0.454	0.813
4	0.679	0.031	2.887	−0.076	0.079	3.385	−0.128	0.142
5	0.699	0.031	2.771	−0.067	0.066	3.184	−0.108	0.111
6	0.652	0.032	2.815	−0.071	0.071	3.261	−0.116	0.122
7	0.684	0.031	2.746	−0.063	0.064	3.144	−0.097	0.105
8	0.773	0.032	3.284	−0.151	0.172	4.240	−0.349	0.549
Praesepe								
9	0.901	0.034	2.799	−0.094	0.106	3.292	−0.138	0.161
10	0.622	0.030	2.827	−0.099	0.112	3.341	−0.149	0.179
11	0.820	0.039	3.543	−0.337	0.548	5.953	−1.223	8.634
12	0.812	0.034	2.972	−0.130	0.148	3.655	−0.230	0.287
13	0.857	0.023	3.058	−0.153	0.174	3.926	−0.290	0.421
14	0.759	0.032	3.179	−0.183	0.221	4.151	−0.400	0.696
15	0.751	0.034	3.282	−0.206	0.260	4.457	−0.524	1.048
16	0.722	0.027	3.045	−0.146	0.167	3.901	−0.272	0.386
17	0.740	0.021	3.130	−0.160	0.188	4.060	−0.328	0.502
18	0.759	0.027	3.223	−0.189	0.232	4.233	−0.447	0.801
19	0.746	0.027	3.200	−0.175	0.210	4.190	−0.397	0.654
NGC2516								
20	0.926	0.106	5.856	−1.133	3.679	8.672	−2.774	99.90
21	1.008	0.071	5.269	−0.837	1.899	6.732	−1.511	5.739
22	0.970	0.045	6.766	−1.541	7.174	13.99	−5.870	99.90
23	1.075	0.078	6.492	−1.415	5.640	12.35	−4.929	99.90
NGC3532								
24	0.482	0.081	3.132	−0.252	0.369	3.450	−0.340	0.563
25	0.563	0.157	3.085	−0.243	0.348	3.409	−0.321	0.523

Table 6—Continued

ID	$M_f[M_\odot]$	$\sigma(M_f)$	OV models			non-OV models		
			$M_i[M_\odot]$	$\sigma_-(M_i)$	$\sigma_+(M_i)$	$M_i[M_\odot]$	$\sigma_-(M_i)$	$\sigma_+(M_i)$
26	0.708	0.157	3.466	-0.399	0.620	3.975	-0.560	1.316
NGC2099 (M37); [Fe/H] = 0.09								
27	0.690	0.095	3.934	-0.248	0.326	4.746	-0.491	0.868
28	0.759	0.131	4.372	-0.436	0.940	6.009	-1.110	6.012
29	0.864	0.164	6.307	-1.557	99.90	99.90	99.90	99.90
30	0.821	0.137	4.666	-0.567	1.891	7.628	-2.020	99.90
31	0.877	0.200	5.497	-1.099	99.90	99.90	99.90	99.90
32	0.614	0.048	4.689	-0.437	0.693	7.806	-1.834	8.624
33	0.742	0.044	4.153	-0.238	0.305	5.187	-0.593	1.015
34	0.959	0.065	4.198	-0.274	0.382	5.323	-0.691	1.433
35	0.561	0.074	5.680	-1.022	4.981	99.90	99.90	99.90
36	0.783	0.051	4.471	-0.364	0.519	6.574	-1.206	3.976
37	0.448	0.126	8.210	-2.545	99.90	99.90	99.90	99.90
38	0.818	0.065	99.90	99.90	99.90	99.90	99.90	99.90
NGC2168 (M35)								
39	0.884	0.079	5.209	-0.595	0.928	6.119	-0.915	1.695
40	0.849	0.050	5.111	-0.522	0.796	5.936	-0.784	1.330
41	0.820	0.055	4.903	-0.387	0.605	5.468	-0.550	0.890
42	0.845	0.040	4.899	-0.385	0.602	5.461	-0.549	0.885
43	0.928	0.040	5.767	-0.862	1.670	7.312	-1.527	4.464
44	0.955	0.041	5.804	-0.869	1.669	7.383	-1.558	4.441
Sirius B								
45	0.978	0.016	5.934	-1.139	3.904	5.426	-0.777	1.198
NGC7789								
46	0.601	0.029	1.853	-0.096	0.128	1.954	-0.072	0.105
47	0.637	0.038	1.864	-0.100	0.132	1.971	-0.078	0.116
48	0.543	0.059	1.871	-0.101	0.134	1.983	-0.083	0.125
NGC6819								
49	0.540	0.020	1.736	-0.090	0.117	1.852	-0.073	0.077
50	0.566	0.022	1.770	-0.097	0.130	1.887	-0.072	0.096

Table 6—Continued

ID	$M_\mathrm{f}[M_\odot]$	$\sigma(M_\mathrm{f})$	OV models			non-OV models		
			$M_\mathrm{i}[M_\odot]$	$\sigma_-(M_\mathrm{i})$	$\sigma_+(M_\mathrm{i})$	$M_\mathrm{i}[M_\odot]$	$\sigma_-(M_\mathrm{i})$	$\sigma_+(M_\mathrm{i})$
NGC1039								
51	0.863	0.075	4.124	-0.364	0.514	5.382	-0.717	1.369
52	0.899	0.076	4.319	-0.435	0.659	6.069	-1.006	2.652
53	0.834	0.074	3.835	-0.279	0.348	4.607	-0.386	0.511
NGC2099 (M37); [Fe/H] $= -0.20$								
27	0.690	0.095	2.994	-0.133	0.145	3.643	-0.269	0.349
28	0.759	0.131	3.123	-0.196	0.259	4.029	-0.443	0.947
29	0.864	0.163	3.522	-0.355	1.056	5.248	-1.460	99.90
30	0.821	0.137	3.232	-0.233	0.374	4.226	-0.570	1.727
31	0.877	0.201	3.424	-0.325	1.085	4.814	-1.064	99.90
32	0.614	0.047	3.239	-0.173	0.200	4.238	-0.486	0.844
33	0.742	0.043	3.055	-0.128	0.144	3.823	-0.273	0.382
34	0.959	0.065	3.068	-0.139	0.156	3.865	-0.306	0.443
35	0.561	0.074	3.454	-0.282	0.412	4.923	-1.010	4.628
36	0.783	0.051	3.174	-0.162	0.181	4.121	-0.408	0.645
37	0.448	0.125	3.628	-0.361	0.628	6.066	-2.242	99.90
38	0.818	0.066	5.529	-1.125	9.156	99.90	99.90	99.90

[a]Values for initial masses equal to $99.90\,M_\odot$ flag those cases where the central value of the progenitor age t_prog, is negative. Similarly, error values of 99.90 indicate that progenitor ages deviating 1-σ from the central value t_prog are negative and as a consequence 1-σ values for M_i cannot be obtained.
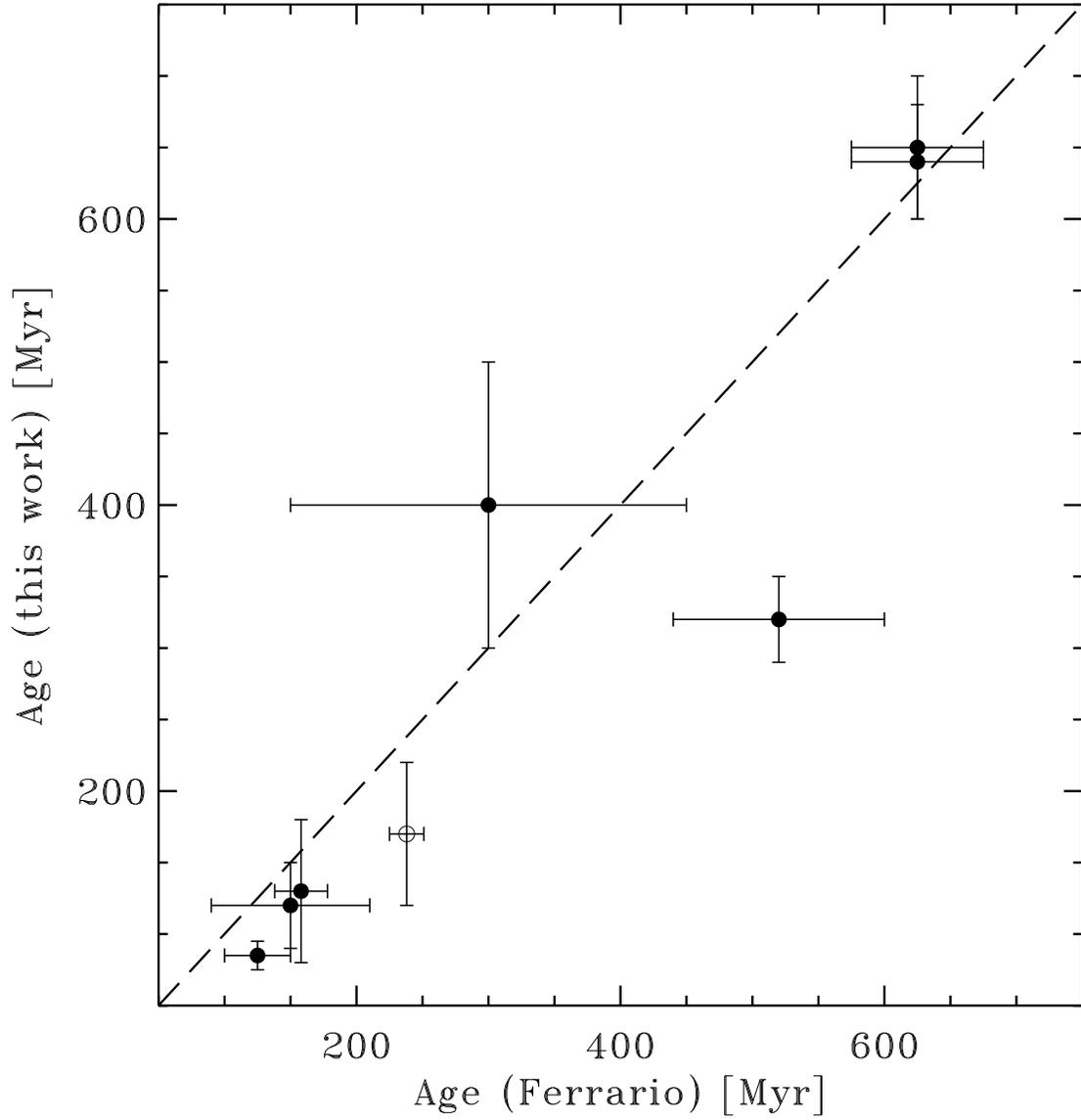
Fig. 1.— Comparison of the cluster ages determined with the BaSTI overshooting isochrones, with the ages adopted from the literature by Ferrario et al. (2005), for the clusters in common. The dashed line displays the 1:1 relation, and the errors are those given by Ferrario et al. (2005) or as listed from Table 3. The open circle shows the results for Sirius A.
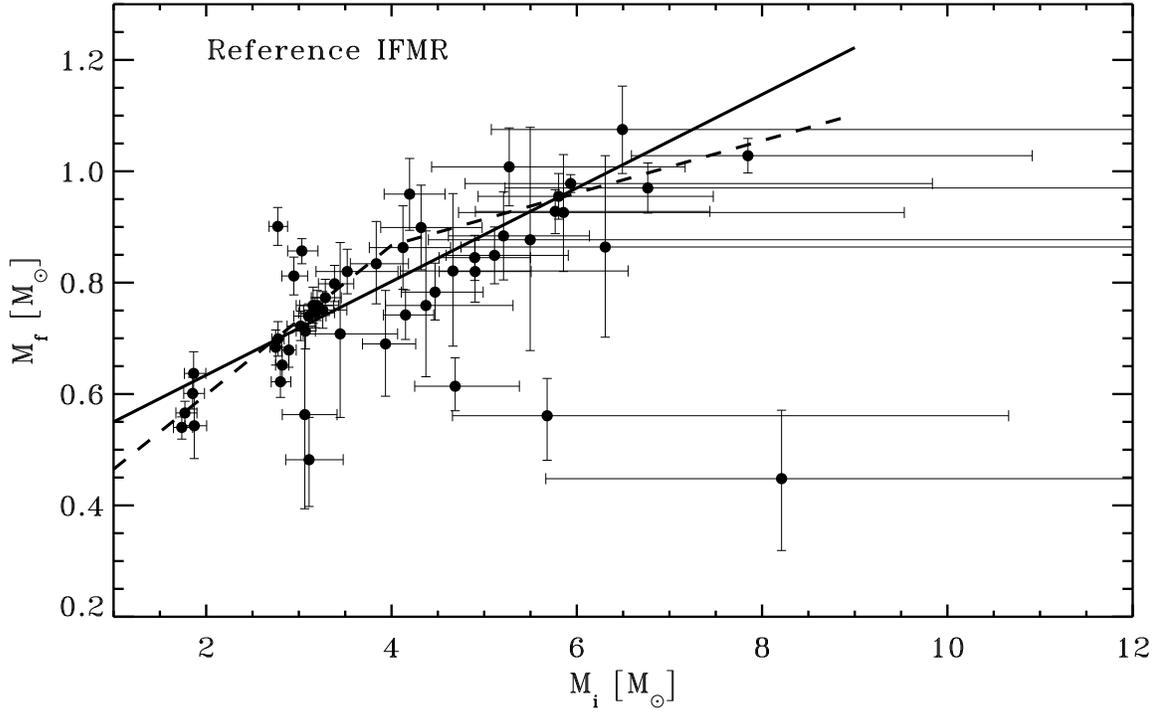
Fig. 2.— Reference IFMR obtained employing BaSTI isochrones and progenitor models with core overshooting together with S00 WD tracks. Lines show fits to the data: the solid line is a linear fit, the dashed line a piecewise linear fit. The pivot point at 4 $M_{\odot}$ has been chosen following theoretical predictions from BaSTI models, that show changes in the slope of the IFMR around those mass values.
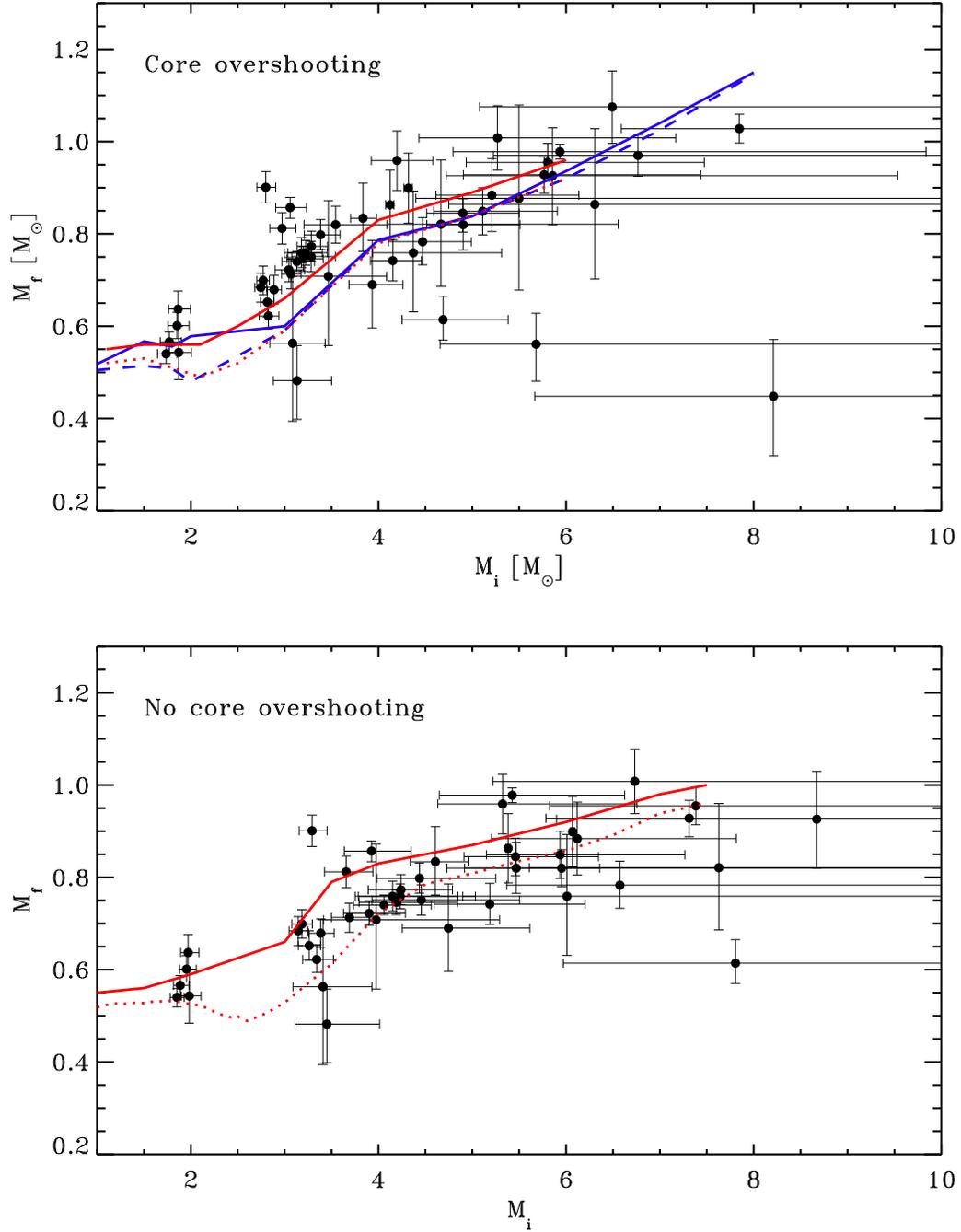
Fig. 3.— Inferred and theoretical IFMRs. Top panel: results for models and isochrones with core overshooting. Solid lines correspond to theoretical IFMRs derived from BaSTI models (thick lines – for [Fe/H]=0.06) and LPCODE models (thin line – for [Fe/H]= 0.06). The dotted thick line shows the $M_i - M_{c1TP}$ relation for BaSTI models and the dashed thin line shows the counterpart from LPCODE models. Bottom panel: results corresponding to models and isochrones without core overshooting. In this case only theoretical results for BaSTI models are shown.
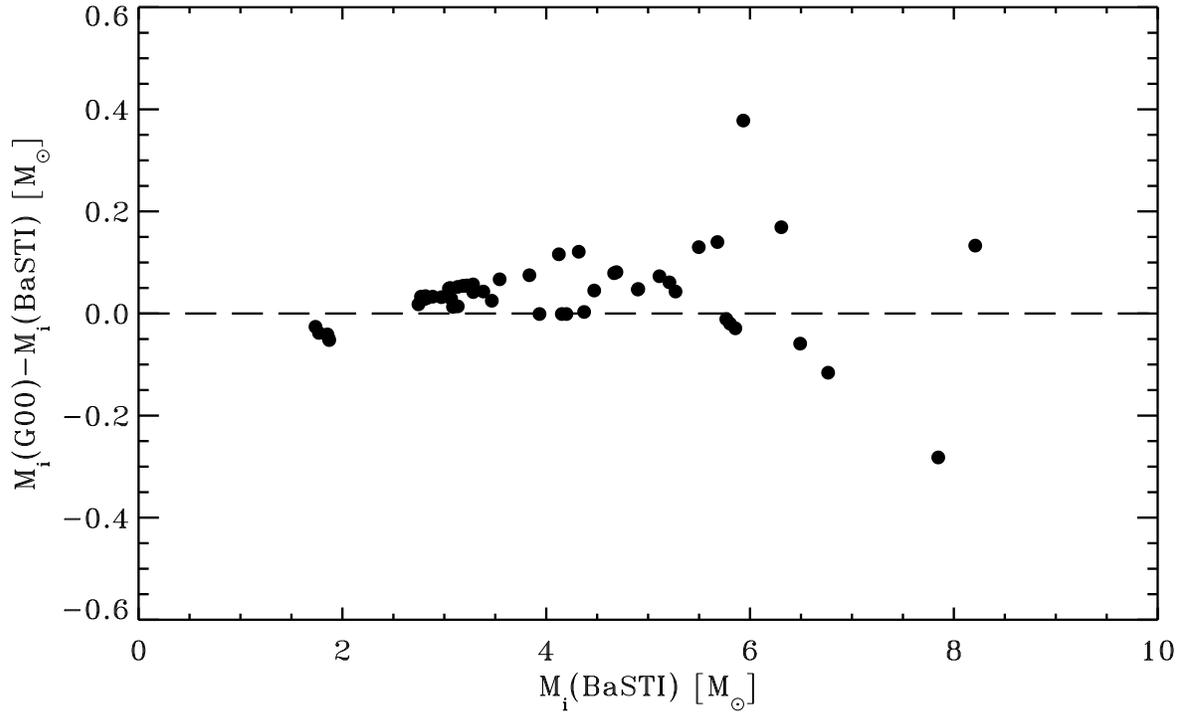
Fig. 4.— Difference between initial masses obtained employing the Padua and BaSTI isochrones and models versus initial masses obtained with BaSTI isochrones and models. Both sets include overshooting treated with different formulations, but giving similar mass extensions of the core overshooting regions at fixed total stellar mass. S00 WD tracks have been used in both cases.
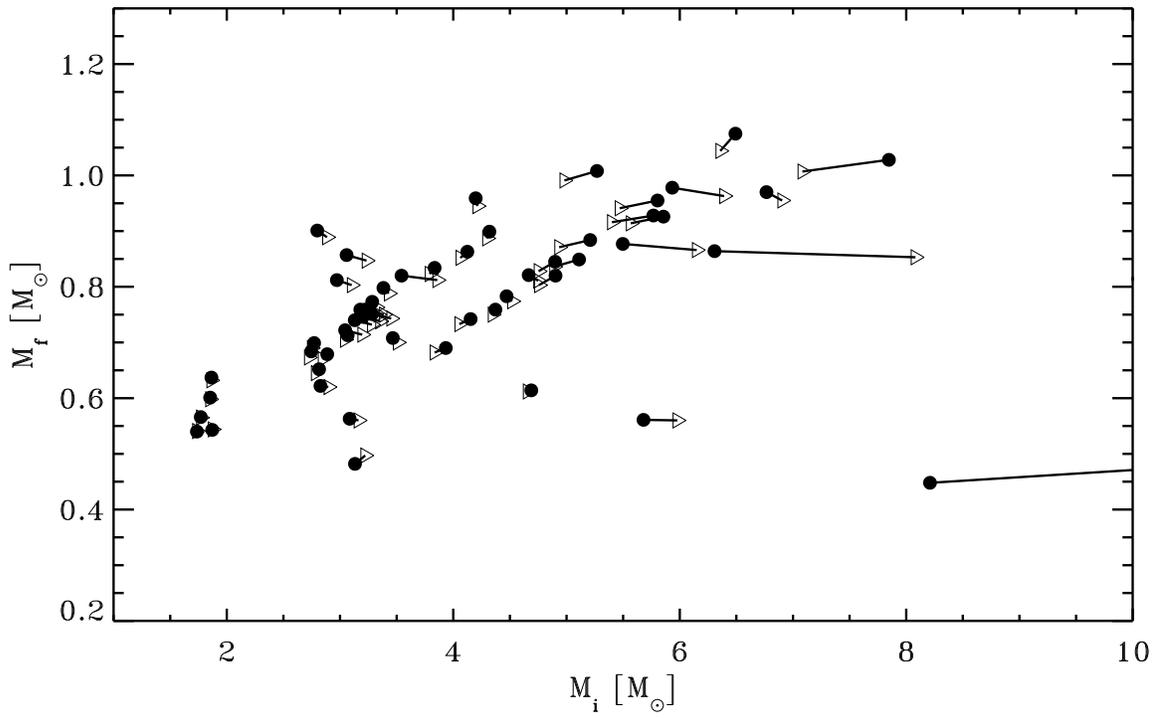
Fig. 5.— Comparison between IFMRs obtained using the S00 (dots) and the LPCODE (triangles) WD tracks. BaSTI isochrones and progenitor models with core overshooting have been used in both cases. Each pair connected by a line represents the same star.
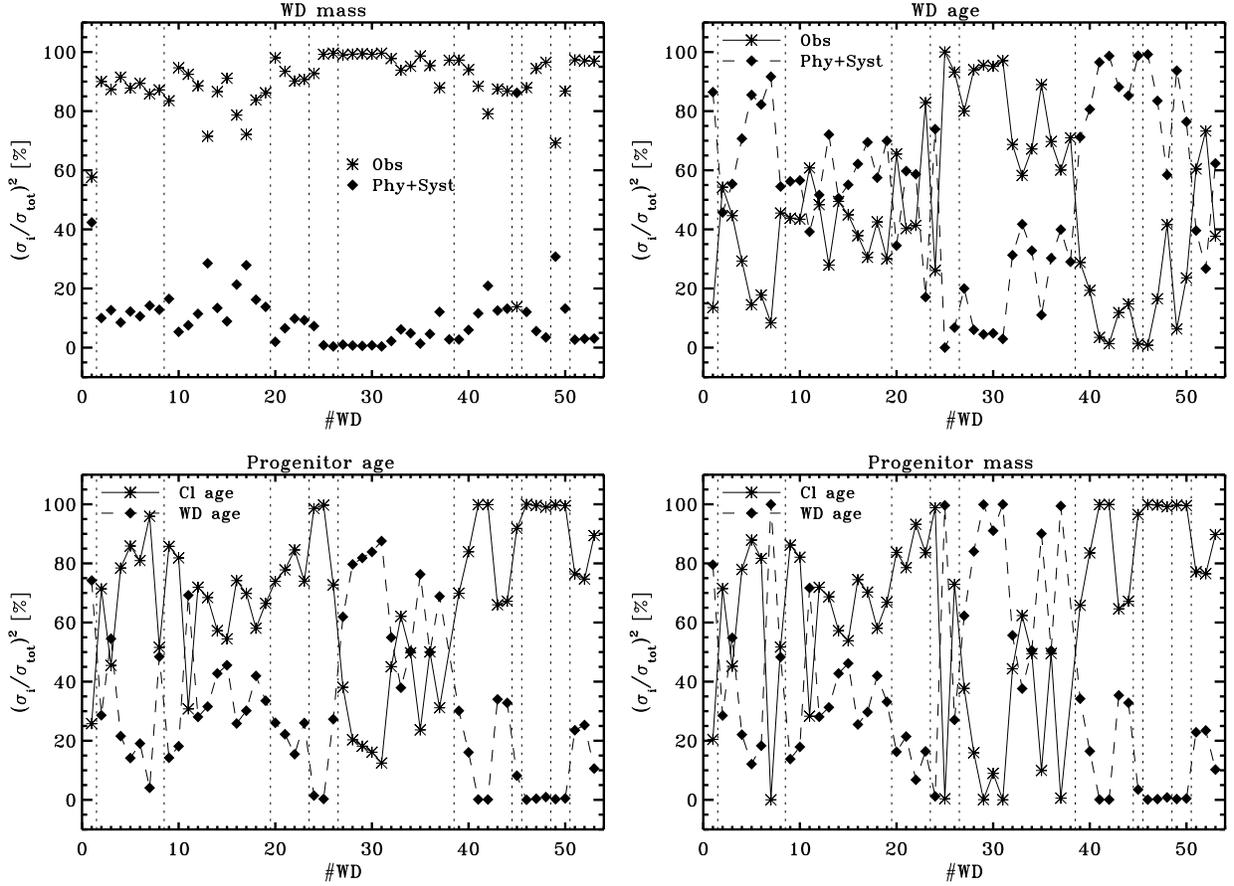
Fig. 6.— Contribution of uncertainty sources to the total error budget for WD mass (upper left), WD age (upper right), progenitor mass (lower left), and progenitor age (lower right panel). The fractional contribution to total sigma σ due to various error sources is given for each WD. Vertical lines separate clusters. For the WDs we show the importance of observational vs. input physics and systematics (different codes, variation of physics inputs, chemical stratification, envelope thickness) for the progenitors that of cluster and WD age.
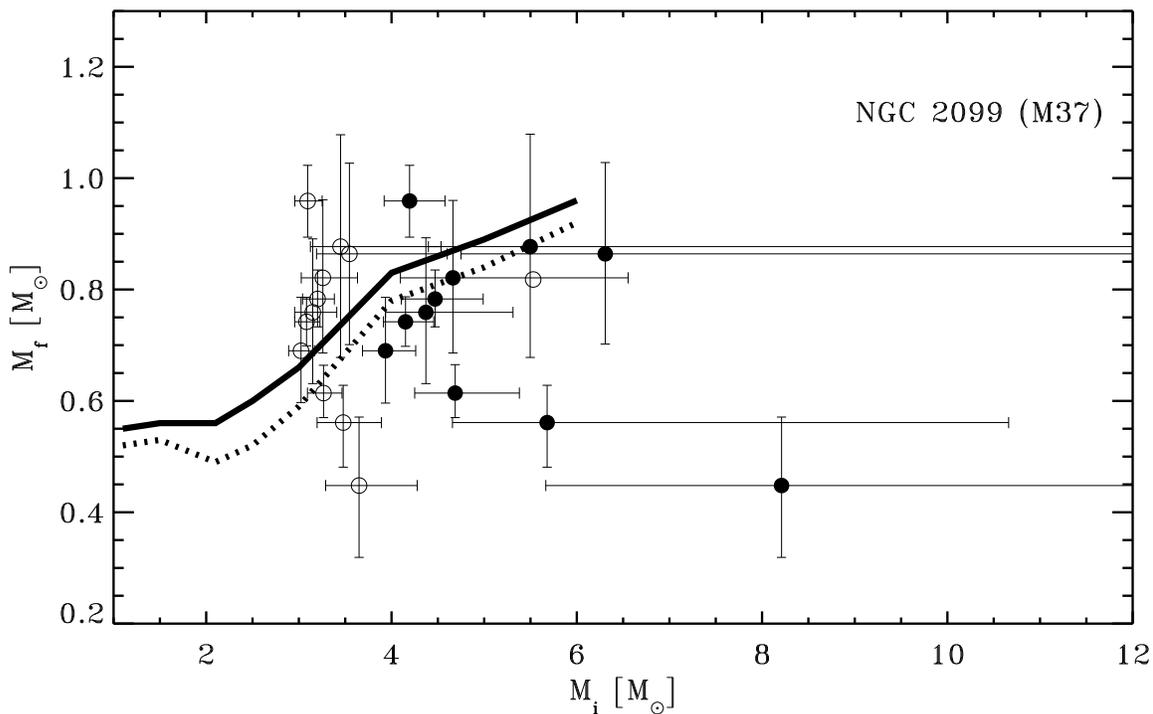
Fig. 7.— IFMR for NGC 2099, for the two [Fe/H] and E(B-V) pairs given in Table 3. Filled circles refer to [Fe/H]= 0.09 and empty circles to [Fe/H]= −0.20. The solid line shows the theoretical IFMR from BaSTI models with core overshooting, the dotted line displays the $M_i - M_{c1TP}$ relation for the same models. Data points lie systematically below the theoretical $M_i - M_{c1TP}$ values when [Fe/H]= 0.09 is adopted.